

An update to the MARVEL dataset and ExoMol line list for $^{12}\text{C}_2$

Laura K. McKemmish,^{1*} Anna-Maree Syme,¹ Jasmin Borsovszky,¹ Sergei N. Yurchenko,²
Jonathan Tennyson,² Tibor Furtenbacher³ and Attila G. Császár³

¹*School of Chemistry, University of New South Wales, 2052 Sydney*

²*Department of Physics and Astronomy, University College London, London WC1E 6BT, United Kingdom*

³*Institute of Chemistry, ELTE Eötvös Loránd University and MTA-ELTE Complex Chemical Systems Research Group, H-1518 Budapest 112, P.O. Box 32, Hungary*

Accepted XXX. Received YYY; in original form ZZZ

ABSTRACT

The spectrum of dicarbon (C_2) is important in astrophysics and for spectroscopic studies of plasmas and flames. The C_2 spectrum is characterized by many band systems with new ones still being actively identified; astronomical observations involve eight of these bands. Recently, Furtenbacher *et al.* (2016, *Astrophys. J. Suppl.*, 224, 44) presented a set of 5699 empirical energy levels for $^{12}\text{C}_2$, distributed among 11 electronic states and 98 vibronic bands, derived from 42 experimental studies and obtained using the MARVEL (Measured Active Rotational-Vibrational Energy Levels) procedure.

Here, we add data from 13 new sources and update data from 5 sources. Many of these data sources characterize high-lying electronic states, including the newly detected $3\ ^3\Pi_g$ state. Older studies have been included following improvements in the MARVEL procedure which allow their uncertainties to be estimated. These older works in particular determine levels in the $\text{C}\ ^1\Pi_g$ state, the upper state of the insufficiently characterized Deslandres–d’Azambuja ($\text{C}\ ^1\Pi_g\text{--A}\ ^1\Pi_u$) band.

The new compilation considers a total of 31 323 transitions and derives 7047 empirical (MARVEL) energy levels spanning 20 electronic and 142 vibronic states. These new empirical energy levels are used here to update the `8states` C_2 ExoMol line list. This updated line list is highly suitable for high-resolution cross-correlation studies in astronomical spectroscopy of, for example, exoplanets, as 99.4% of the transitions with intensities over 10^{-18} cm molecule^{-1} at 1000 K have frequencies determined by empirical energy levels.

Key words: molecular data; opacity; astronomical data bases: miscellaneous; planets and satellites: atmospheres; stars: low-mass; comets: general.

1 INTRODUCTION

The spectroscopy of the dicarbon molecule, C_2 , has a long history. Interestingly, C_2 was originally observed by Wollaston (1802), which represents the pre-history of spectroscopy. This observation was followed by the identification (Swan 1857) of the well-known Swan $d\ ^3\Pi_g\text{--}a\ ^3\Pi_u$ band system. The last decade has seen the spectroscopic characterization of several new bands of C_2 , including the first observation of multiplicity-changing “intercombination” bands linking both the singlet-triplet (Chen *et al.* 2015) and triplet-quintet (Bornhauser *et al.* 2011) states. These observations have allowed the determination of reliable frequencies of singlet-triplet transitions, which are thought to be important in comets (Rousselot *et al.* 2000) and are candidates for observation in the interstellar medium (Lebourlot & Roueff 1986). Detection of triplet-quintet transitions has led to the spectroscopic characterization of

a number of quintet states for the first time (Schmidt & Bacskay 2011; Bornhauser *et al.* 2015, 2017). In addition, recent experiments detected and characterized a number of new triplet bands (Welsh *et al.* 2017; Krechkivska *et al.* 2017).

Astronomically, C_2 is unusual in that it has been studied via a large number of band systems including the Swan, Phillips, Deslandres–d’Azambuja, Ballik–Ramsay, Mulliken and Herzberg-F bands, see Figure 1 for the band designations. The Swan (Swings 1943; Gredel *et al.* 1989; Lambert *et al.* 1990; Rousselot *et al.* 2000) and the Deslandres–d’Azambuja (Gredel *et al.* 1989) band systems have been discovered in the spectra of comets when models of cometary emission have been found to require no less than two singlet, $X\ ^1\Sigma_g^+$ and $A\ ^1\Pi_u$, and four triplet, $a\ ^3\Pi_u$, $b\ ^3\Sigma_g^-$, $c\ ^3\Sigma_u^+$, and $d\ ^3\Pi_g$, electronic states to explain the observations. Indeed, two of the intercombination bands mentioned above, $a\ ^3\Pi_u\text{--}X\ ^1\Sigma_g^+$ and $c\ ^3\Sigma_u^+\text{--}X\ ^1\Sigma_g^+$, are needed to explain the observed intensities in the Swan band (Rousselot *et al.* 2000).

* E-mail: l.mckemmish@unsw.edu.au

C_2 has a strong presence in the solar photosphere where it has been observed using the Swan (Asplund et al. 2005), the Phillips, and the Ballik–Ramsay (Brault et al. 1982) bands. The Phillips and Ballik–Ramsay bands have also been observed in carbon stars (Goebel et al. 1983; Goorvitch 1990), while Swan bands have been observed in peculiar white dwarfs (Hall & Maxwell 2008; Kowalski 2010) and the coronae borealis star V coronae australis (Rao & Lambert 2008).

Interstellar C_2 has been observed via the infrared Phillips band (Gredel et al. 2001; Iglesias-Groth 2011), while the Swan band emissions can be seen in the Red Rectangle (Wehres et al. 2010). Absorption in the Phillips, Mulliken and Herzberg-F bands can be seen in translucent clouds (Sonnentrucker et al. 2007).

These astronomical observations require high-quality laboratory data for their analysis and interpretation. Recent spectroscopic studies have probed new bands with well-known band systems (Nakajima 2019; Krechkivska et al. 2018), providing new data on them. In addition, recent spectroscopic studies on C_2 have used techniques yielding improved ionization (Krechkivska et al. 2016) and dissociation energies (Visser et al. 2019). Theoretical studies also started to provide reliable association rates (Babb et al. 2019). Altogether work on the C_2 molecule remains as lively as ever with the interpretation of its bonding and spectroscopy remaining somewhat as a puzzle to conventional chemical physics (Macrae 2016).

Figure 1 gives an overview of the observed band systems for $^{12}C_2$ with colour used to indicate those explicitly dealt with in this study. In response to the needs of astrophysics and other areas of physics, Yurchenko et al. (2018b) computed a comprehensive line list for $^{12}C_2$ as part of the ExoMol project (Tennyson & Yurchenko 2012), called the 8states line list. This line list was generated by variational solution of the nuclear Schrödinger equation for the states involved (Yurchenko et al. 2016) and covers the band systems linking the lowest eight electronic states, namely the Swan, Phillips, Ballik–Ramsay, Duck, Bernath B and B' bands, and the singlet-triplet intercombination lines. As a precursor to performing these calculations, Furtenbacher et al. (2016) performed a MARVEL (Measured Active Rotational-Vibrational Energy Levels (Császár et al. 2007; Furtenbacher et al. 2007; Furtenbacher & Császár 2012a), see Section 2 for a description) analysis for the $^{12}C_2$ isotopologue. The empirical energies generated by MARVEL were incorporated in the $^{12}C_2$ 8states line list giving, for example, the most accurate predictions available for the singlet-triplet intercombination lines.

A number of advances has led us to review and update the $^{12}C_2$ MARVEL project. First, improvements in the MARVEL procedure, including significantly improved error handling (Tóbiás et al. 2019), was found to influence the results of the original study. Second, while the original MARVEL study considered 42 sources of spectroscopic $^{12}C_2$ data, a number of largely older sources (Dieke & Lochte-Holtgreven 1930; Fox & Herzberg 1937; Herzberg & Sutton 1940; Phillips 1950; Herzberg et al. 1969; Goodwin & Cool 1988, 1989) were not considered in 2016 as they did not contain any uncertainty estimates, a requirement for use in the MARVEL procedure. New combination difference approaches implemented in MARVEL allow these uncertainties to be accurately estimated. These earlier works contain data on states that have not been observed in more recent studies; in particular the studies of 40HeSu (Herzberg & Sutton 1940), 50Phillips (Phillips 1950) and 67Messerle (Messerle 1967) contain the only published high resolution $^{12}C_2$ spectra of the Deslandres–d’Azambuja band. Finally, and most importantly, a series of new studies have provided additional data for known bands (Welsh et al. 2017; Krechkivska

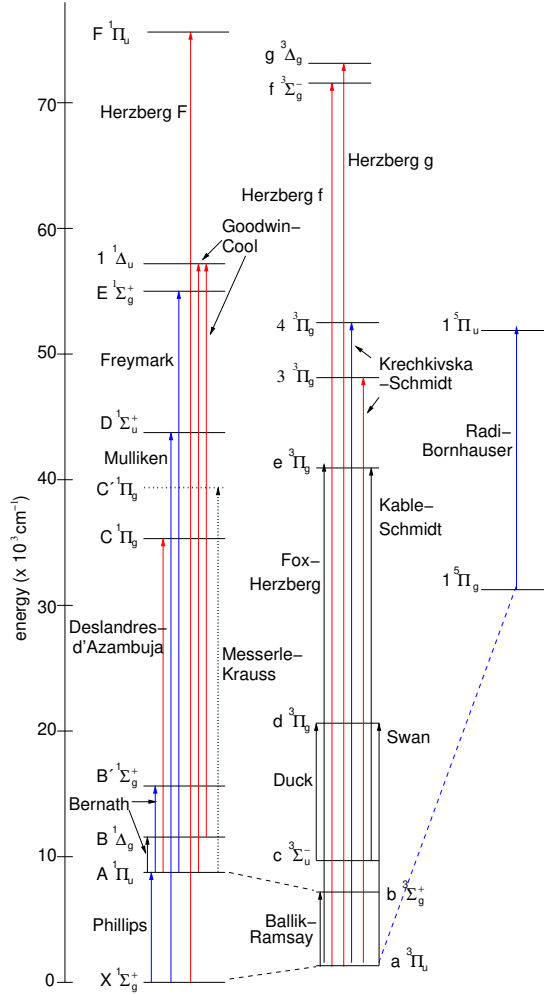


Figure 1. The band system of $^{12}C_2$ with its well-established names. The dashed lines represent observed but unnamed intercombination bands; colours indicate newly considered bands (red) and updates (blue). The Messerle–Krauss band and the associated $C' \ ^1\Pi_g$ state are depicted in dots as doubts have been raised about their correctness.

et al. 2017) and characterized several new bands for the first time (Schmidt & Bacskay 2011; Bornhauser et al. 2015, 2017). These sources are combined with those considered previously to produce an updated set of empirical (MARVEL) rovibronic energy levels during this study. All (new and old) data sources are referenced by band in Table 5 (*vide infra*).

In this work we also present an updated and improved version of the $^{12}C_2$ 8states ExoMol line list, which incorporates the new and extended MARVEL-derived set of empirical energy levels.

2 THE MARVEL PROCEDURE

Details about the MARVEL procedure (Furtenbacher et al. 2007; Furtenbacher & Császár 2012a; Tóbiás et al. 2019), built upon the theory of spectroscopic networks (SN) (Császár & Furtenbacher 2011; Császár et al. 2016), have been given in recent publications (Furtenbacher et al. 2014; Császár et al. 2016; Tóbiás et al. 2019, 2020). Therefore, only a brief discussion is given here.

The MARVEL protocol yields empirical rovibronic energies with well-defined provenance and uncertainties; it starts with the

construction of a SN using the dataset of measured and assigned transitions collated from the literature. Each measured transition must have a *unique* (though not necessarily physically relevant) assignment, which determines its place within the SN, and an uncertainty. What happens next is basically an inversion of the transitions information, yielding empirically determined rovibronic energy levels within each component of the SN. Along this process validation of the experimental information is performed, utilizing several elements of network theory. Recently the algorithms employed by MARVEL have been systematically improved, the relationship of SNs to formal network theory considered (Császár & Furtenbacher 2011; Furtenbacher & Császár 2012b; Árendás et al. 2016), and the underlying methodology reviewed (Furtenbacher et al. 2014; Császár et al. 2016). MARVEL has been used to obtain accurate empirical rovibronic energy levels with statistically sound uncertainties for a considerable number of diatomic molecules of astronomical interest (Furtenbacher et al. 2016; McKemmish et al. 2017; Darby-Lewis et al. 2018; Yurchenko et al. 2018a; McKemmish et al. 2018; Darby-Lewis et al. 2019a,b; Furtenbacher et al. 2019). These MARVEL energy levels are crucial to enabling the generation of MARVELised line lists (e.g. McKemmish et al. (2019)) suitable for high-resolution cross-correlation studies of low-signal objects such as exoplanets (e.g. Birkby et al. (2013)).

3 UPDATED MARVEL SET OF ASSIGNED TRANSITIONS

3.1 Overview

We have updated the MARVEL set of assigned transitions for $^{12}\text{C}_2$ through the inclusion of 13 new data sources (8 new sources from prior to the original update and 5 post-2016 sources) and through the revision of transitions from six further data sources. The number of included transitions has risen from the 2016 values of 23 251 (22 937 validated) to 31 323 (30 792 validated).

We usually added new data to the pre-existing MARVEL set of transitions and uncertainties, unless specified otherwise. The uncertainties used for each source were usually taken from the original paper, but increased as required, first for internal self-consistency of the data within a single data source and then for self-consistency with the full MARVEL compilation of data.

The parity-defining quantum numbers used in the original compilation are not necessary given that lambda-doubling transitions have not been observed in $^{12}\text{C}_2$, and have thus been removed in the present study for simplicity.

The new transitions file thus has the format shown in Table 1. The transitions file serves as both input to the MARVEL procedure and as a single consolidated source of assigned transition frequencies and uncertainties for $^{12}\text{C}_2$.

Salient details of each source of new and updated experimental data are summarised in Tables 2 to 4, which specify, for each included vibronic band, (1) the number of total and validated transitions, (2) the average and maximum uncertainty of the spectral lines after self-consistency, and (3) the J and the wavenumber ranges of the transitions. The same details are provided in the supplementary information for transitions retained from the original MARVEL compilation (Furtenbacher et al. 2016).

3.2 New data sources, pre-2016

The 2016 original MARVEL compilation of $^{12}\text{C}_2$ spectroscopic data did not incorporate sources that either (a) did not include an esti-

mate of the transition frequency uncertainty, or (b) involved very high-lying electronic states, e.g., $\text{C } ^1\Pi_g$, $\text{F } ^1\Pi_u$, $\text{f } ^3\Sigma_g^+$, and $\text{g } ^3\Delta_g$.

Many of these new data sources include transitions in the ultra-violet and have much higher uncertainties than other data sources. In most data sources, we limited the maximum uncertainty to 0.5 cm^{-1} . Next, we provide information about these sources one by one.

30DiLo (Dieke & Lochte-Holtgreven 1930) An early source of Deslandres–d’Azambuja ($\text{C } ^1\Pi_g - \text{A } ^1\Pi_u$) transitions for low-energy vibrational states, which have surprisingly not been remeasured for $^{12}\text{C}_2$ despite the high uncertainties of these data. Uncertainties were estimated using combination differences based on the use of lower-state energy levels determined by MARVEL, the estimated source uncertainties are 0.2 cm^{-1} .

37FoHe (Fox & Herzberg 1937) The first measurements of the Fox–Herzberg ($\text{e } ^3\Pi_g - \text{a } ^3\Pi_u$) band, all with upper vibrational state of $v = 0$. Uncertainties were estimated using combination differences based on the use of lower-state energies determined by MARVEL, the estimated source uncertainties are 0.2 cm^{-1} . Two of these bands, (0–3) and (0–6), have not been remeasured, though all involved energy levels are now well understood by other band measurements.

40HeSu (Herzberg & Sutton 1940) Another source of Deslandres–d’Azambuja ($\text{C } ^1\Pi_g - \text{A } ^1\Pi_u$) transitions with a number of vibrational bands. Uncertainties were estimated using combination differences based on the use of lower-state energies determined by MARVEL, the estimated source uncertainties are 0.2 cm^{-1} .

50Phillips (Phillips 1950) Even another source of Deslandres–d’Azambuja ($\text{C } ^1\Pi_g - \text{A } ^1\Pi_u$) transitions, with significantly excited vibrational states involved.

67Messerle (Messerle 1967) Some data from Messerle’s 1967 thesis was located (Nauta 2020); these data are relevant for the Deslandres–d’Azambuja ($\text{C } ^1\Pi_g - \text{A } ^1\Pi_u$) band. Note that no data from the putative Messerle–Krauss bands ($\text{C}' ^1\Pi_g - \text{A } ^1\Pi_u$) were found.

69HeLaMa (Herzberg et al. 1969) These data are the sole source for many very high-lying bands, located above $70\,000 \text{ cm}^{-1}$. Uncertainties were estimated using combination differences based on the use of lower-state energies determined by MARVEL, the estimated source uncertainties are 0.1 cm^{-1} , with blended lines given a starting uncertainty of 0.2 cm^{-1} . Lines with recommended MARVEL uncertainties higher than 0.5 cm^{-1} were not validated; this process only removed a small number of lines and all bands mostly consisted of validated lines.

88GoCo (Goodwin & Cool 1988) To ensure reliable inclusion of the 88GoCo (Goodwin & Cool 1988), and in fact 89GoCo (Goodwin & Cool 1989), data (the only source of data for the $1^1\Delta_u$ state), uncertainties up to 2 cm^{-1} were required to be permitted in these two sources. These high uncertainty values can be attributed to the quality of the early ultraviolet studies, which have a stated absolute energy error of 2 cm^{-1} , though the relative uncertainties were stated as $\pm 0.2 \text{ cm}^{-1}$.

89GoCo (Goodwin & Cool 1989) Following the considerations of 88GoCo (Goodwin & Cool 1988), an earlier paper by the same authors, uncertainties for the 89GoCo data were initially set as 0.2 cm^{-1} , but allowed to increase as required; all transitions were validated with uncertainties less than 1.2 cm^{-1} .

Table 1. Extract from the 12C-12C_2020update.marvel.inp input file for $^{12}\text{C}_2$.

1	2	3	4	5	6	7	8	9	10	11
$\tilde{\nu}$	$\Delta\tilde{\nu}$	State'	v'	J'	F'	State''	v''	J''	F''	ID
3345.6527	0.006132865	B ¹ Deltag	1	9	1	A ¹ Piu	1	10	1	16ChKaBeTa.167
3347.987	0.0093071	b ³ Sigmat-	4	26	3	a ³ Piu	5	26	3	15ChKaBeTa.1594
3349.659	0.009250366	B ¹ Deltag	1	16	1	A ¹ Piu	1	16	1	16ChKaBeTa.168
3349.8868	0.0015	B ¹ Deltag	0	30	1	A ¹ Piu	0	31	3	88DoNiBeb.125
3350.6451	0.007	b ³ Sigmat-	4	27	2	a ³ Piu	5	27	2	15ChKaBeTa.1582
3351.6007	0.003	B ¹ Deltag	1	8	1	A ¹ Piu	1	9	1	16ChKaBeTa.169
3352.8642	0.003	B ¹ Deltag	0	39	1	A ¹ Piu	0	39	1	16ChKaBeTa.170
3354.5954	0.003	B ¹ Deltag	1	15	1	A ¹ Piu	1	15	1	16ChKaBeTa.171
3356.9124	0.007	b ³ Sigmat-	4	14	3	a ³ Piu	5	15	3	15ChKaBeTa.1557
3357.1991	0.003176643	B ¹ Deltag	1	7	1	A ¹ Piu	1	8	1	16ChKaBeTa.172

Column	Notation	
1	$\tilde{\nu}$	Transition frequency (in cm^{-1})
2	$\Delta\tilde{\nu}$	Estimated uncertainty in transition frequency (in cm^{-1})
3	State'	Electronic state of upper energy level; also includes parity for Π states and Ω for triplet states
4	v'	Vibrational quantum number of upper level
5	J'	Total angular momentum of upper level
6	F'	Spin multiplet component of upper level, labelled in energy order
7	State''	Electronic state of lower energy level; also includes parity for Π states and Ω for triplet states
8	v''	Vibrational quantum number of lower level
9	J''	Total angular momentum of lower level
10	F''	Spin multiplet component of lower level, labelled in energy order
11	ID	Unique ID for transition, with reference key for source and counting number

3.3 New data sources, post-2016

17BoViBeKn (Bornhauser et al. 2017) This paper provides new data on the quintet bands and three assignments of the quintet-triplet spin-forbidden bands. However, two of these three new spin-forbidden bands were inconsistent with the rest of the MARVEL compilation without uncertainties of around 2.4 cm^{-1} and were thus excluded; in contrast, 67 spin-forbidden transitions between the same two electronic states in 11BoSyKnGe (Bornhauser et al. 2011) all validated with smaller uncertainties.

17WeKrNaBa (Welsh et al. 2017) Rotationally cool experimental conditions enabled detailed study of low- J ultraviolet rovibronic transitions in the Fox–Herzberg ($e^3\Pi_g - a^3\Pi_u$) band. No explicit uncertainty was provided in this paper; an estimated source uncertainty of 0.035 cm^{-1} was used, though this seems to be a slight underestimation based on the uncertainties MARVEL found.

17KrWeBaNa (Krechivska et al. 2017) This is the first study of the $3^3\Pi_g$ state, observed via the $3^3\Pi_g - a^3\Pi_u$ transitions, with the paper also substantially expanding on previously known data on the $4^3\Pi_g$ state. The estimated source uncertainties are 0.035 cm^{-1} . Detailed MARVEL-based analyses of the data revealed that the original assignments were not self-consistent within this paper. Following these analyses, one of the original authors identified (Nauta 2020) a calibration error in the $4^3\Pi_g - a^3\Pi_u$ ($0-5$) transition frequencies, which can be corrected by decreasing all frequencies in this band by 0.9 cm^{-1} . Though it could not be confirmed, a calibration error was also suspected in the $4^3\Pi_g - a^3\Pi_u$ ($1-3$) transition frequencies; the MARVEL analysis showed the data set became self-consistent without unreasonably large uncertainties if these transition frequencies were decreased by 1.0 cm^{-1} .

18KrWeFrNa (Krechivska et al. 2018) Rotationally cool experimental conditions enabled the detailed study of low- J rovibronic transitions in the Mulliken ($D^1\Sigma_u^+ - X^1\Sigma_g^+$) $\Delta v = \pm 2$ sequence.

This paper does not present explicit uncertainties for the spectral lines. Given the ultraviolet frequency of these transitions, an estimated source uncertainty of 0.02 cm^{-1} was assigned, with reasonable results.

19Nakajima (Nakajima 2019) The paper provides an estimate for the line uncertainties as 0.01 cm^{-1} , which we adopted as the estimated source uncertainty.

3.4 Corrections to the 2016 compilation

During the process of updating the compilation of $^{12}\text{C}_2$ rovibronic data, a number of issues with the original data were identified and corrected. A source-by-source specification of the corrections follows.

48Phillips (Phillips 1948b) A small number of digitisation errors were identified and corrected following a thorough re-examination of the band structure.

49Phillips (Phillips 1949) Significant errors with quantum numbers, including incorrect band assignments, were identified and corrected, and the repetition of one band's data identified and removed.

86HaWi (Hardwick & Winicur 1986) The 2016 compilation included only 100 of the spectral lines reported in this paper; the other 497 lines have been added to this update.

07TaHiAm (Tanabashi et al. 2007) The original data compilation included 3813 transitions, but some of these transitions were calculated rather than measured and many measured transitions were excluded. The source was reprocessed into MARVEL format, giving a total of 4813 transitions, with calculated transitions (labelled “z”) excluded, blended lines given a starting uncertainty of 0.01 cm^{-1} and well resolved isolated lines given an estimated source uncertainty of 0.005 cm^{-1} . Note that the data from the 02TaAm (Tanabashi & Amano 2002) source that was reproduced in 07TaHiAm

Table 2. Newly included data sources (tags in bold). Given are details of the vibronic band, the vibrational states (Vib.) and the total angular momentum quantum numbers (J) involved, the number of transitions (Trans.) validated (V) and original accessed (A), the wavenumber (Wn) range of the band, and information about source uncertainties (Unc.), with their average (Av) and maximum (Max) values.

Band	Vib.	J -range	Trans. (V/A)	Wn range (cm^{-1})	Unc. (cm^{-1}) (Av/Max)
30DiLo (Dieke & Lochte-Holtgreven 1930)					
$\text{C } ^1\Pi_g - \text{A } ^1\Pi_u$	(0-0)	1-73	143/143	25 952-27 066	0.202/0.350
$\text{C } ^1\Pi_g - \text{A } ^1\Pi_u$	(0-1)	1-86	153/158	24 370-25 722	0.194/0.200
$\text{C } ^1\Pi_g - \text{A } ^1\Pi_u$	(1-0)	1-71	133/138	27 714-28 617	0.205/0.432
$\text{C } ^1\Pi_g - \text{A } ^1\Pi_u$	(1-1)	6-64	107/111	26 132-26 981	0.205/0.500
$\text{C } ^1\Pi_g - \text{A } ^1\Pi_u$	(1-2)	1-72	136/136	24 574-25 690	0.201/0.349
$\text{C } ^1\Pi_g - \text{A } ^1\Pi_u$	(2-1)	3-67	122/124	27 825-28 575	0.202/0.332
$\text{C } ^1\Pi_g - \text{A } ^1\Pi_u$	(2-3)	7-54	83/88	24 734-25 375	0.194/0.450
37FoHe (Fox & Herzberg 1937)					
$\text{e } ^3\Pi_g - \text{a } ^3\Pi_u$	(0-3)	5-43	176/182	34 445-35 025	0.310/0.642
$\text{e } ^3\Pi_g - \text{a } ^3\Pi_u$	(0-4)	3-47	212/230	32 798-33 487	0.373/0.684
$\text{e } ^3\Pi_g - \text{a } ^3\Pi_u$	(0-5)	22-45	87/90	31 300-31 689	0.274/0.500
$\text{e } ^3\Pi_g - \text{a } ^3\Pi_u$	(0-6)	17-37	63/75	30 011-30 301	0.247/0.638
40HeSu (Herzberg & Sutton 1940)					
$\text{C } ^1\Pi_g - \text{A } ^1\Pi_u$	(3-1)	1-24	45/45	29 419-29 577	0.207/0.291
$\text{C } ^1\Pi_g - \text{A } ^1\Pi_u$	(4-2)	1-36	68/68	29 289-29 504	0.200/0.200
$\text{C } ^1\Pi_g - \text{A } ^1\Pi_u$	(5-3)	1-35	56/56	28 910-29 899	0.200/0.200
$\text{C } ^1\Pi_g - \text{A } ^1\Pi_u$	(5-4)	1-32	62/62	27 439-27 632	0.200/0.200
$\text{C } ^1\Pi_g - \text{A } ^1\Pi_u$	(6-5)	1-41	73/79	26 714-27 100	0.185/0.200
50Phillips (Phillips 1950)					
$\text{C } ^1\Pi_g - \text{A } ^1\Pi_u$	(7-6)	1-37	64/64	26 954-27 229	0.200/0.200
67Messele (Messele 1967)					
$\text{C } ^1\Pi_g - \text{A } ^1\Pi_u$	(5-4)	1-53	103/103	27 231-27 632	0.029/0.092
69HeLaMa (Herzberg et al. 1969)					
$\text{F } ^1\Pi_u - \text{X } ^1\Sigma_g^+$	(0-0)	10-38	42/42	74 153-74 550	0.121/0.256
$\text{F } ^1\Pi_u - \text{X } ^1\Sigma_g^+$	(1-0)	2-34	38/38	75 812-76 102	0.141/0.484
$\text{f } ^3\Sigma_g^+ - \text{a } ^3\Pi_u$	(0-0)	3-32	111/113	69 974-70 208	0.152/0.480
$\text{f } ^3\Sigma_g^+ - \text{a } ^3\Pi_u$	(1-0)	2-34	113/115	71 232-71 538	0.159/0.500
$\text{f } ^3\Sigma_g^+ - \text{a } ^3\Pi_u$	(2-0)	2-26	95/100	72 611-72 840	0.178/0.500
$\text{g } ^3\Delta_g - \text{a } ^3\Pi_u$	(0-0)	3-32	202/230	71 467-71 674	0.114/0.500
$\text{g } ^3\Delta_g - \text{a } ^3\Pi_u$	(1-0)	3-31	199/206	72 978-73 128	0.141/0.500
88GoCo (Goodwin & Cool 1988)					
$\text{I } ^1\Delta_u - \text{A } ^1\Pi_u$	(0-0)	2-28	66/66	48 796-49 126	0.659/1.841
$\text{I } ^1\Delta_u - \text{A } ^1\Pi_u$	(0-1)	2-30	94/94	47 148-47 547	1.032/2.161
$\text{I } ^1\Delta_u - \text{A } ^1\Pi_u$	(0-2)	2-33	121/121	45 604-45 988	0.435/1.475
$\text{I } ^1\Delta_u - \text{A } ^1\Pi_u$	(0-3)	2-26	67/67	44 118-44 457	0.503/1.180
$\text{I } ^1\Delta_u - \text{A } ^1\Pi_u$	(0-4)	1-21	88/88	42 708-42 949	0.702/1.079
$\text{I } ^1\Delta_u - \text{A } ^1\Pi_u$	(1-0)	3-34	88/88	49 850-50 231	0.380/1.144
$\text{I } ^1\Delta_u - \text{A } ^1\Pi_u$	(1-1)	2-37	125/125	48 194-48 650	0.566/1.355
$\text{I } ^1\Delta_u - \text{A } ^1\Pi_u$	(1-2)	2-32	88/88	46 803-47 093	0.418/1.266
$\text{I } ^1\Delta_u - \text{A } ^1\Pi_u$	(1-3)	2-28	78/79	45 210-45 551	0.761/1.342
$\text{I } ^1\Delta_u - \text{A } ^1\Pi_u$	(1-4)	3-28	48/48	43 791-44 040	0.672/1.502
$\text{I } ^1\Delta_u - \text{A } ^1\Pi_u$	(2-0)	2-31	102/102	50 873-51 287	0.399/1.370
$\text{I } ^1\Delta_u - \text{A } ^1\Pi_u$	(2-1)	3-28	53/53	49 538-49 708	1.087/1.879
$\text{I } ^1\Delta_u - \text{A } ^1\Pi_u$	(2-4)	2-19	56/56	44 926-45 111	0.873/1.643
89GoCo (Goodwin & Cool 1989)					
$\text{I } ^1\Delta_u - \text{B } ^1\Delta_g$	(0-1)	2-29	60/60	43 973-44 140	0.658/1.223

was not included. Given the high resolution of the data, transitions with uncertainties greater than 0.2 cm^{-1} were deemed misassignments and not validated (though they are still in the included MARVEL file with a "-" in front of the transition frequency, as usual); in total 88 transitions were not validated, mostly at the beginning or end of a given band. When processing these data to determine optimal uncertainties, the 48Phillips (Phillips 1948b) and 49Phillips (Phillips 1949) data were removed before being re-added; this ensured the more recent data had a larger number of valid transitions with lower uncertainties than the older data.

16ChKaBeTa (Chen et al. 2016) Due to late inclusion of this data source, the lines from the $\text{B } ^1\Sigma_g^+ - \text{A } ^1\Pi_u$ band were missed during the original compilation; these 104 missing lines have been added in this update.

Additionally, for 06PeSi (Petrova & Sinitsa 2006), we want to note that we retained the 2016 MARVEL values, but that these were

Table 3. New experimental data sources for $^{12}\text{C}_2$ which appeared since the original MARVEL study (Furtenbacher et al. 2016) was published. Details as in Table 2.

Band	Vib.	J -range	Trans. (V/A)	Wn range (cm^{-1})	Unc. (cm^{-1}) (Av/Max)
17BoViBeKn (Bornhauser et al. 2017)					
$\text{I } ^5\Pi_g - \text{a } ^3\Pi_u$	(3-6)	4-4	1/3	22 733-22 733	0.018/0.055
$\text{I } ^5\Pi_u - \text{I } ^3\Pi_g$	(1-0)	1-6	11/11	22 601-22 632	0.055/0.055
$\text{d } ^3\Pi_g - \text{a } ^3\Pi_u$	(8-6)	1-10	39/41	22 722-22 774	0.092/0.302
17WeKrNaBa (Welsh et al. 2017)					
$\text{e } ^3\Pi_g - \text{a } ^3\Pi_u$	(0-2)	1-17	112/112	36 472-36 641	0.047/0.208
$\text{e } ^3\Pi_g - \text{a } ^3\Pi_u$	(1-3)	1-13	118/118	35 969-36 105	0.067/0.258
$\text{e } ^3\Pi_g - \text{a } ^3\Pi_u$	(10-0)	0-12	67/67	48 331-48 461	0.060/0.309
$\text{e } ^3\Pi_g - \text{a } ^3\Pi_u$	(2-2)	1-13	80/80	38 536-38 652	0.078/0.194
$\text{e } ^3\Pi_g - \text{a } ^3\Pi_u$	(2-3)	1-15	115/115	36 932-37 082	0.058/0.222
$\text{e } ^3\Pi_g - \text{a } ^3\Pi_u$	(3-4)	1-13	124/124	36 316-36 466	0.054/0.264
$\text{e } ^3\Pi_g - \text{a } ^3\Pi_u$	(4-0)	1-16	160/160	43 486-43 689	0.060/0.213
$\text{e } ^3\Pi_g - \text{a } ^3\Pi_u$	(5-0)	0-15	131/131	44 346-44 550	0.048/0.257
$\text{e } ^3\Pi_g - \text{a } ^3\Pi_u$	(5-3)	0-8	51/51	39 697-39 767	0.070/0.188
$\text{e } ^3\Pi_g - \text{a } ^3\Pi_u$	(6-0)	0-16	116/116	45 210-45 381	0.066/0.239
$\text{e } ^3\Pi_g - \text{a } ^3\Pi_u$	(6-3)	1-10	43/43	40 526-40 598	0.091/0.249
$\text{e } ^3\Pi_g - \text{a } ^3\Pi_u$	(7-0)	0-12	94/94	46 030-46 186	0.053/0.184
$\text{e } ^3\Pi_g - \text{a } ^3\Pi_u$	(8-0)	1-15	121/121	46 754-46 967	0.056/0.189
$\text{e } ^3\Pi_g - \text{a } ^3\Pi_u$	(9-0)	0-14	98/98	47 570-47 724	0.056/0.160
17KrWeBa (Krechivskaja et al. 2017)					
$\text{I } ^3\Pi_g - \text{a } ^3\Pi_u$	(3-2)	2-7	29/29	46 842-46 894	0.108/0.160
$\text{I } ^3\Pi_g - \text{a } ^3\Pi_u$	(3-5)	1-8	41/41	42 183-42 252	0.116/0.313
$\text{I } ^3\Pi_g - \text{a } ^3\Pi_u$	(8-3)	2-7	9/9	49 181-49 205	0.180/0.373
$\text{I } ^3\Pi_g - \text{a } ^3\Pi_u$	(8-4)	1-6	19/19	47 596-47 655	0.170/0.286
$\text{I } ^3\Pi_g - \text{a } ^3\Pi_u$	(8-5)	2-6	11/11	46 084-46 133	0.110/0.136
$\text{I } ^3\Pi_g - \text{a } ^3\Pi_u$	(8-6)	1-9	24/24	44 583-44 633	0.238/0.456
$\text{I } ^3\Pi_g - \text{a } ^3\Pi_u$	(0-2)	2-7	17/17	48 272-48 327	0.230/0.490
$\text{I } ^3\Pi_g - \text{a } ^3\Pi_u$	(0-3)	2-8	24/24	46 683-46 756	0.184/0.351
$\text{I } ^3\Pi_g - \text{a } ^3\Pi_u$	(0-4)	2-7	13/14	45 165-45 208	0.238/0.345
$\text{I } ^3\Pi_g - \text{a } ^3\Pi_u$	(0-5)	1-9	20/20	43 617-43 686	0.220/0.447
$\text{I } ^3\Pi_g - \text{a } ^3\Pi_u$	(0-6)	1-8	13/13	42 137-42 184	0.147/0.340
$\text{I } ^3\Pi_g - \text{a } ^3\Pi_u$	(1-2)	3-8	16/21	49 544-49 593	0.213/0.349
$\text{I } ^3\Pi_g - \text{a } ^3\Pi_u$	(1-3)	2-7	18/18	47 973-48 023	0.197/0.421
$\text{I } ^3\Pi_g - \text{a } ^3\Pi_u$	(1-4)	2-6	12/13	46 425-46 473	0.317/0.500
$\text{I } ^3\Pi_g - \text{a } ^3\Pi_u$	(1-5)	2-7	20/26	44 900-44 951	0.121/0.297
$\text{I } ^3\Pi_g - \text{a } ^3\Pi_u$	(2-3)	1-7	25/25	49 257-49 328	0.147/0.302
$\text{I } ^3\Pi_g - \text{a } ^3\Pi_u$	(2-5)	2-7	21/21	46 220-46 270	0.127/0.288
18KrWeFrNa (Krechivskaja et al. 2018)					
$\text{D } ^1\Sigma_g^+ - \text{X } ^1\Sigma_g^+$	(4-2)	1-23	17/17	46 537-46 667	0.020/0.020
$\text{D } ^1\Sigma_g^+ - \text{X } ^1\Sigma_g^+$	(5-3)	1-19	15/15	46 519-46 611	0.022/0.032
$\text{D } ^1\Sigma_g^+ - \text{X } ^1\Sigma_g^+$	(6-4)	1-11	12/12	46 431-46 511	0.035/0.083
$\text{D } ^1\Sigma_g^+ - \text{X } ^1\Sigma_g^+$	(7-5)	1-11	12/12	46 355-46 433	0.039/0.074
$\text{D } ^1\Sigma_g^+ - \text{X } ^1\Sigma_g^+$	(8-6)	1-11	9/13	46 291-46 361	0.024/0.030
$\text{D } ^1\Sigma_g^+ - \text{X } ^1\Sigma_g^+$	(9-7)	1-13	12/12	46 228-46 302	0.020/0.020
$\text{D } ^1\Sigma_g^+ - \text{X } ^1\Sigma_g^+$	(10-8)	1-11	12/12	46 167-46 243	0.021/0.025
$\text{D } ^1\Sigma_g^+ - \text{X } ^1\Sigma_g^+$	(11-9)	1-11	12/12	46 130-46 205	0.021/0.028
19Nakajima (Nakajima 2019)					
$\text{A } ^1\Pi_u - \text{X } ^1\Sigma_g^+$	(10-4)	1-30	43/43	15 588-15 882	0.005/0.022
$\text{A } ^1\Pi_u - \text{X } ^1\Sigma_g^+$	(10-5)	1-25	35/35	13 991-14 175	0.005/0.022
$\text{A } ^1\Pi_u - \text{X } ^1\Sigma_g^+$	(11-4)	1-21	26/26	17 103-17 220	0.005/0.017
$\text{A } ^1\Pi_u - \text{X } ^1\Sigma_g^+$	(11-5)	1-23	29/29	15 379-15 513	0.005/0.022
$\text{A } ^1\Pi_u - \text{X } ^1\Sigma_g^+$	(6-0)	1-28	40/40	17 152-17 417	0.017/0.132
$\text{A } ^1\Pi_u - \text{X } ^1\Sigma_g^+$	(6-1)	1-26	36/36	15 378-15 590	0.012/0.130
$\text{A } ^1\Pi_u - \text{X } ^1\Sigma_g^+$	(9-4)	1-31	43/43	14 236-14 520	0.004/0.012

reassigned from the original paper's assignments because the original contained unphysical assignments for the quantum numbers of homonuclear diatomics.

3.5 Discussion

The spread of uncertainties for every data source used for the updated MARVEL input is shown in Figure 2. The horizontal axis goes through each data source in chronological order. The colours of the data are assigned to the electronic bands of the transition, ordered by transitions frequency. This plot clearly shows that for each source there are a significant number of transitions with uncertainties above the minimum uncertainty for that data set; these uncertainty increases were required to ensure self-consistency with the data coming from other sources. The figure makes it also clear that

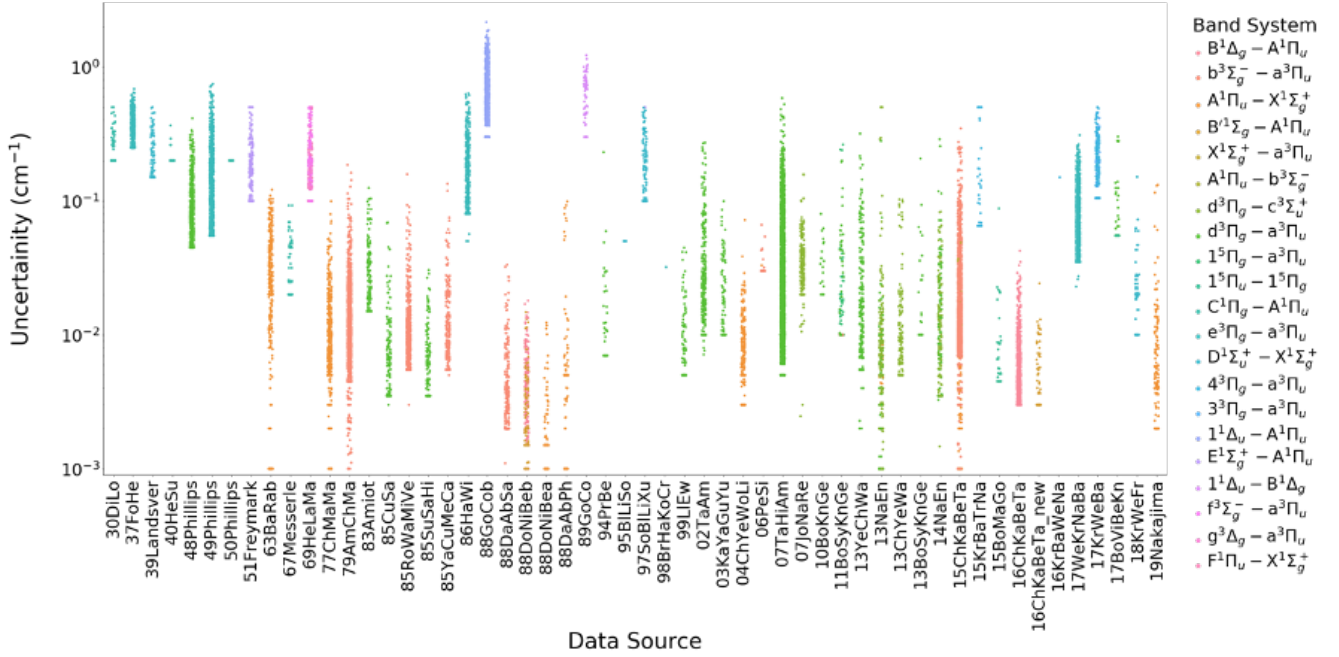


Figure 2. The range of transition frequency uncertainties for every source involved in the full MARVEL input file. See Table 5 for the citations to these sources.

pre-1960 sources have much larger uncertainties than the later data, though there is no clear trend in improved accuracy since 1960. Most data sources since 1960 have minimum uncertainties between 10^{-3} to 10^{-2} cm^{-1} . The post-1960 outliers with higher uncertainties, on the order of 0.1 cm^{-1} , are usually very-high-frequency transitions in the ultraviolet region. These higher uncertainties are expected as this region is more spectrally congested and UV instruments are more expensive with lower spectral resolution than visible instruments due to decreased market demand.

Colours in Figure 1, *vide supra*, demonstrate that the new data sources added to the $^{12}\text{C}_2$ MARVEL compilation in this paper increase the number of bands considered from 11 to 21, with updates in data available for 7 of the originally included bands. The specific experimental sources in our MARVEL compilation for each electronic transition band system are detailed in Table 5. It is clear that some band systems, especially the $b^3\Sigma_g^- - a^3\Pi_u$, $d^3\Pi_g - a^3\Pi_u$, $e^3\Pi_g - a^3\Pi_u$, $A^1\Pi_u - X^1\Sigma_g^+$ ones, have been extensively explored with thousands of measured transitions in up to 16 different publications. These heavily explored band systems are strong absorption bands in astrophysical environments. In contrast, some other systems have data only from a single paper. The triplet manifold is generally better explored than the singlet manifold, despite the fact that the electronic ground state of C_2 is a singlet. The number of quintet and spin-forbidden intersystem lines remains quite small, but the latter in particular are very important for setting the relative energies of the singlet, triplet, and quintet manifolds accurately.

Table 5 also provides details about the number of unique versus total transitions measured. The high number of unique versus total transitions in these data clearly demonstrates that most re-examinations of a particular band system produce data for different vibronic bands rather than re-measuring existing data at a higher accuracy. This result emphasises the need for a centrally-collated

source of all available experimental data in one consistent format, as provided by this paper.

With these new included data, every observed band has MARVEL-compiled rotationally-resolved data with two exceptions: the Kable–Schmidt (Nakajima et al. 2009) $e^3\Pi_g - c^3\Sigma_u^+$ band around $40\,000$ cm^{-1} and the Messerle–Krauss (Messerle & Krauss 1967) $C'^1\Pi_g - A^1\Pi_u$ band around $30\,000$ cm^{-1} . Initial errors in the e state constants prohibited a good fit to the Kable–Schmidt band in 2009; new constants (Welsh et al. 2017) obtained from better data in the Fox–Herzberg band allowed a much better fit of the $e^3\Pi_g - c^3\Sigma_u^+$ (4–3) band in that paper’s supplementary information, although a full experimental assigned line list was not produced. In the case of the Messerle–Krauss band, recent unpublished investigations (Nauta & Schmidt 2020) suggests that the observed lines of the Messerle–Krauss band are actually part of the Deslandres–d’Azambuja ($C^1\Pi_g - A^1\Pi_u$) band and that the true $C'^1\Pi_g$ is much higher in energy, as consistently predicted by *ab initio* theory.

The full MARVEL input file with formatted assigned transitions includes 31 323 transitions with 6 quantum numbers following the formatting of the original C_2 MARVEL transitions file. It is provided as supplementary information with the latest update available online on MARVELOnline, <http://kkrk.chem.elte.hu/marvelonline/>.

4 UPDATED MARVEL DATA

4.1 Spectroscopic Network

The experimental spectroscopic network of $^{12}\text{C}_2$ built from assigned transitions has one main component with 7047 energy levels, incorporating 2061 singlet, 4910 triplet, and 76 quintet states. These energy levels span 20 electronic states and 142 vibronic levels. There are 203 other spectroscopic networks, none of which

Table 4. Updates to previously included data sources. Details as in Table 2.

Band	Vib.	J- range	Trans. (V/A)	Wn range (cm^{-1})	Unc. (cm^{-1}) (Av/Max)
<i>48Phillips</i> (minor corrections) (Phillips 1948a)					
$d^3\Pi_{g^-} - a^3\Pi_u$	(0–2)	1–53	247/247	16152–16751	0.056/0.275
$d^3\Pi_{g^-} - a^3\Pi_u$	(1–3)	2–56	228/230	16332–16690	0.066/0.288
$d^3\Pi_{g^-} - a^3\Pi_u$	(10–9)	0–43	194/196	20697–20957	0.065/0.297
$d^3\Pi_{g^-} - a^3\Pi_u$	(2–4)	11–42	153/153	16498–16864	0.079/0.254
$d^3\Pi_{g^-} - a^3\Pi_u$	(3–5)	1–30	110/110	16662–16868	0.073/0.338
$d^3\Pi_{g^-} - a^3\Pi_u$	(8–6)	5–32	114/117	22648–22812	0.074/0.414
$d^3\Pi_{g^-} - a^3\Pi_u$	(9–8)	15–43	124/128	20962–21198	0.080/0.268
<i>49Phillips</i> (re-processed) (Phillips 1949)					
$e^3\Pi_{g^-} - a^3\Pi_u$	(0–2)	6–39	166/172	35963–36596	0.144/0.632
$e^3\Pi_{g^-} - a^3\Pi_u$	(1–2)	4–55	234/266	36506–37635	0.099/0.709
$e^3\Pi_{g^-} - a^3\Pi_u$	(1–3)	3–52	226/259	35091–36064	0.129/0.728
$e^3\Pi_{g^-} - a^3\Pi_u$	(2–1)	5–43	198/203	39453–40202	0.100/0.746
$e^3\Pi_{g^-} - a^3\Pi_u$	(2–2)	4–49	234/235	37643–38608	0.081/0.534
$e^3\Pi_{g^-} - a^3\Pi_u$	(2–3)	8–35	129/129	36618–37032	0.120/0.440
$e^3\Pi_{g^-} - a^3\Pi_u$	(3–1)	4–41	185/188	40429–41127	0.101/0.652
$e^3\Pi_{g^-} - a^3\Pi_u$	(3–2)	15–48	148/149	38595–39370	0.103/0.654
$e^3\Pi_{g^-} - a^3\Pi_u$	(4–1)	5–44	196/197	41174–42019	0.096/0.611
<i>86HaWi</i> (extended) (Hardwick & Winicur 1986)					
$e^3\Pi_{g^-} - a^3\Pi_u$	(0–4)	2–39	192/197	33035–33502	0.174/0.500
$e^3\Pi_{g^-} - a^3\Pi_u$	(0–5)	2–38	219/221	31386–31977	0.098/0.413
$e^3\Pi_{g^-} - a^3\Pi_u$	(1–8)	2–31	171/179	28195–28580	0.104/0.446
<i>07TaHiAm</i> (re-processed) (Tanabashi et al. 2007)					
$d^3\Pi_{g^-} - a^3\Pi_u$	(0–0)	1–87	411/417	19355–20602	0.005/0.047
$d^3\Pi_{g^-} - a^3\Pi_u$	(0–1)	0–38	191/191	17740–18085	0.007/0.030
$d^3\Pi_{g^-} - a^3\Pi_u$	(0–2)	1–38	171/171	16147–16514	0.006/0.018
$d^3\Pi_{g^-} - a^3\Pi_u$	(1–0)	0–53	214/215	21104–21587	0.008/0.041
$d^3\Pi_{g^-} - a^3\Pi_u$	(1–1)	0–52	174/174	19490–19999	0.008/0.041
$d^3\Pi_{g^-} - a^3\Pi_u$	(1–2)	0–29	138/138	17899–18117	0.008/0.040
$d^3\Pi_{g^-} - a^3\Pi_u$	(10–9)	1–36	160/160	20749–20958	0.005/0.042
$d^3\Pi_{g^-} - a^3\Pi_u$	(2–0)	2–34	118/118	22814–23044	0.014/0.075
$d^3\Pi_{g^-} - a^3\Pi_u$	(2–1)	0–40	84/86	21202–21514	0.007/0.022
$d^3\Pi_{g^-} - a^3\Pi_u$	(2–2)	3–36	51/51	19612–19910	0.007/0.053
$d^3\Pi_{g^-} - a^3\Pi_u$	(2–3)	0–37	63/63	18043–18349	0.009/0.040
$d^3\Pi_{g^-} - a^3\Pi_u$	(3–1)	1–35	170/170	22869–23109	0.025/0.117
$d^3\Pi_{g^-} - a^3\Pi_u$	(3–2)	2–39	159/161	21282–21573	0.012/0.054
$d^3\Pi_{g^-} - a^3\Pi_u$	(3–3)	1–30	139/139	19715–19933	0.015/0.096
$d^3\Pi_{g^-} - a^3\Pi_u$	(3–4)	1–29	40/41	18172–18359	0.009/0.061
$d^3\Pi_{g^-} - a^3\Pi_u$	(3–5)	0–31	137/137	16648–16846	0.007/0.039
$d^3\Pi_{g^-} - a^3\Pi_u$	(3–6)	0–30	129/130	15149–15390	0.008/0.055
$d^3\Pi_{g^-} - a^3\Pi_u$	(4–3)	2–43	119/119	21339–21647	0.008/0.096
$d^3\Pi_{g^-} - a^3\Pi_u$	(4–5)	3–25	65/65	18276–18441	0.011/0.081
$d^3\Pi_{g^-} - a^3\Pi_u$	(4–6)	3–25	66/66	16777–16968	0.011/0.093
$d^3\Pi_{g^-} - a^3\Pi_u$	(5–4)	0–37	191/192	21368–21615	0.015/0.102
$d^3\Pi_{g^-} - a^3\Pi_u$	(5–5)	20–20	1/1	19984–19984	0.005/0.005
$d^3\Pi_{g^-} - a^3\Pi_u$	(5–6)	0–32	88/88	18353–18584	0.007/0.027
$d^3\Pi_{g^-} - a^3\Pi_u$	(5–7)	1–20	42/42	16879–17004	0.006/0.014
$d^3\Pi_{g^-} - a^3\Pi_u$	(6–5)	0–37	136/138	21360–21594	0.007/0.049
$d^3\Pi_{g^-} - a^3\Pi_u$	(6–8)	0–26	52/52	16946–17129	0.007/0.053
$d^3\Pi_{g^-} - a^3\Pi_u$	(7–6)	2–37	135/136	21297–21523	0.009/0.178
$d^3\Pi_{g^-} - a^3\Pi_u$	(7–9)	1–25	93/93	16970–17121	0.007/0.031
$d^3\Pi_{g^-} - a^3\Pi_u$	(8–6)	3–26	91/91	22666–22824	0.009/0.063
$d^3\Pi_{g^-} - a^3\Pi_u$	(8–7)	0–14	35/36	21228–21311	0.012/0.085
$d^3\Pi_{g^-} - a^3\Pi_u$	(9–8)	0–37	172/172	20990–21208	0.006/0.050
<i>16ChKaBeTa</i> (new lines) (Chen et al. 2016)					
$B^1\Sigma_g^+ - A^1\Pi_u$	(4–3)	0–28	35/35	7798–7949	0.004/0.013
$B^1\Sigma_g^+ - A^1\Pi_u$	(4–5)	2–30	39/39	4790–4958	0.004/0.024
$B^1\Sigma_g^+ - A^1\Pi_u$	(4–6)	2–26	30/30	3400–3501	0.006/0.013

have more than 12 energy levels. Therefore, they are not considered further in this paper.

Figure 3 visually demonstrates the connectivity of the experimental spectroscopic network of $^{12}\text{C}_2$. In all of the subfigures, the nodes are the energy levels, and the edges are the transitions between them. The three subfigures show the SN at the resolution of electronic (top), vibronic (middle) and rovibronic (bottom) states, with the same colour scheme used for all figures.

The top sub-figure of Figure 3 shows that the singlet and triplet manifolds are largely independent, as expected, with two different spin-forbidden bands connecting the manifolds. The quintet manifold is connected to the whole spectroscopic network *via* transitions between the $1^5\Pi_g$ and a $^3\Pi_u$ states. Most of the triplet-bands studied have a $^3\Pi_u$ as the lower-energy state, whereas for the singlet

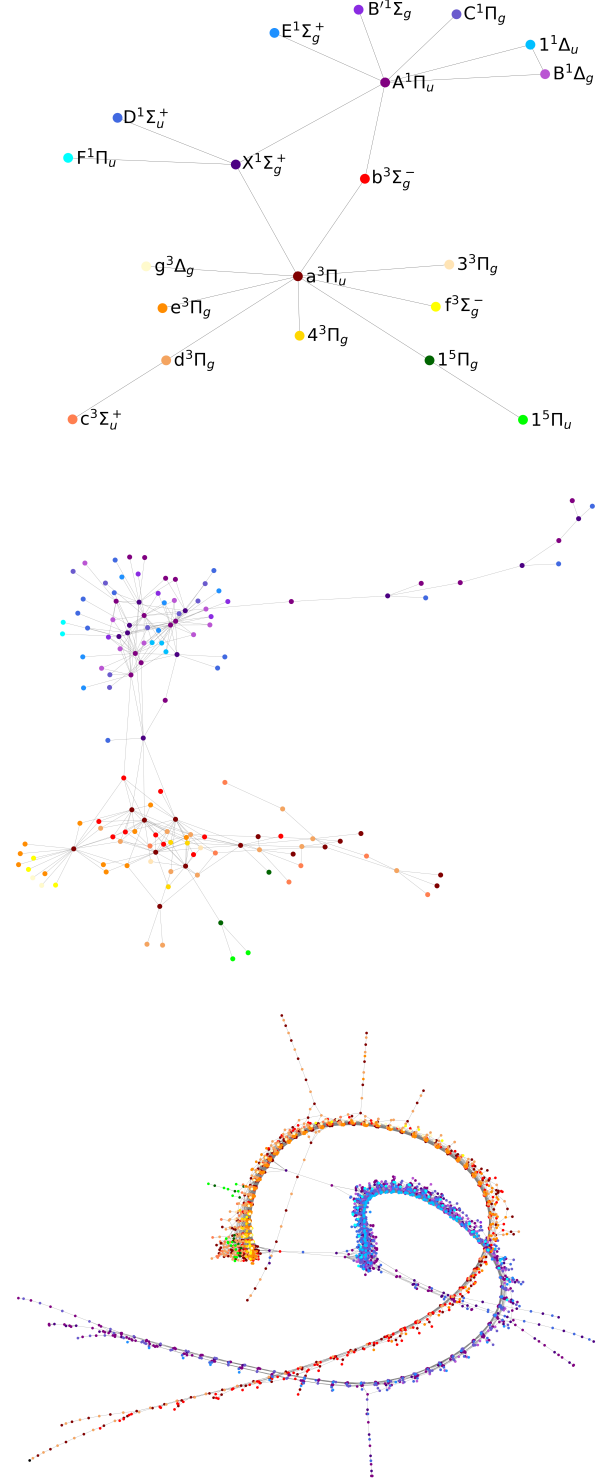


Figure 3. Spectroscopic networks of $^{12}\text{C}_2$ produced using the MARVEL input and output data. Each electronic state is given a colour which is labelled in top subfigure (network of electronic states) and repeated in middle subfigure (network of vibronic states) and bottom subfigure (network of rovibronic states). The bluer colours are singlets, the redder colours are triplets and the green colours are quintets.

Table 5. All experimental data sources of rotationally-resolved assigned transitions (Trans.) for all investigated band system in $^{12}\text{C}_2$, where Tot refers to the total number of transitions and Uniq refers to the number of unique transitions. Bold band names indicate bands newly included in this update, while italicized names indicate pre-existing bands with new data. Bold sources are newly included in this 2020 MARVEL update, italicised sources are updated from the previous 2016 MARVEL compilation.

Multiplicity	Band name	Band System	Trans. (Tot/Uniq)	Sources
Singlet				
	<i>Phillips</i>	$A^1\Pi_u - X^1\Sigma_g^+$	2729/2248	63BaRab (Ballik & Ramsay 1963), 77ChMaMa (Chauville et al. 1977), 88DaAbPh (Davis et al. 1988), 88DoNiBea (Douay et al. 1988a), 04ChYeWoLi (Chan et al. 2004), 06PeSi (Petrova & Sinita 2006), 13NaEn (Nakajima & Endo 2013), 15ChKaBeTa (Chen et al. 2015), 19Nakajima (Nakajima 2019)
	Bernath B	$B^1\Delta_g - A^1\Pi_u$	1508/1508	88DoNiBeb (Douay et al. 1988b), 16ChKaBeTa (Chen et al. 2016)
	<i>Bernath B'</i>	$B'^1\Sigma_g^+ - A^1\Pi_u$	341/341	88DoNiBeb (Douay et al. 1988b), <i>16ChKaBeTa</i> (Chen et al. 2016)
	Deslandres-d'Azambuja	$C^1\Pi_g - A^1\Pi_u$	1375/1375	30DiLo (Dieke & Lochte-Holtgreven 1930), 40HeSu (Herzberg & Sutton 1940), 50Phillips (Phillips 1950), 67Messerle (Messerle 1967)
	<i>Mulliken</i>	$D^1\Sigma_u^+ - X^1\Sigma_g^+$	464/299	39Landsver (Landsverk 1939), 95BILiSo (Blunt et al. 1995), 97SoBILiXu (Kaminski et al. 1997), 18KrWeFrNa (Krechivska et al. 2018)
	Freymark	$E^1\Sigma_u^+ - A^1\Pi_u$	442/442	51Freymark (Freymark 1951), 97SoBILiXu (Sorkhabi et al. 1997)
	Herzberg F	$F^1\Pi_u - a^3\Pi_u$	80/80	69HeLaMa (Herzberg et al. 1969)
	Goodwin-Cool	$1^1\Delta_u - A^1\Pi_u$	1075/1075	88GoCo (Goodwin & Cool 1988)
	Goodwin-Cool	$1^1\Delta_u - B^1\Delta_g$	60/60	89GoCo (Goodwin & Cool 1989)
Triplet				
	Ballik-Ramsay	$b^3\Sigma_g^- - a^3\Pi_u$	7813/5739	79AmChMa (Amiot et al. 1979), 85RoWaMiVe (Roux et al. 1985), 85YaCuMeCa (Yan et al. 1985), 88DaAbSa (Davis et al. 1988), 06PeSi (Petrova & Sinita 2006), 11BoSyKnGe (Bornhauser et al. 2011), 15ChKaBeTa (Chen et al. 2015)
	<i>Swan</i>	$d^3\Pi_g - a^3\Pi_u$	8518/6585	48Phillips (Phillips 1948a), 83Amiot (Amiot 1983), 85CuSa (Curtis & Sarre 1985), 85SuSaHi (Suzuki et al. 1985), 94PrBe (Prasad & Bernath 1994), 99LIEW (Lloyd & Ewart 1999), 02TaAm (Tanabashi & Amano 2002), 03KaYaGuYu (Kaniki et al. 2003), 07TaHiAm (Tanabashi et al. 2007), 10BoKnGe (Bornhauser et al. 2010), 11BoSyKnGe (Bornhauser et al. 2011), 13BoSyKnGe (Bornhauser et al. 2013), 13NaEn (Nakajima & Endo 2013), 13YeChWa (Yeung et al. 2013), 14NaEn (Nakajima & Endo 2014), 17BoViBeKn (Bornhauser et al. 2017)
	Duck	$d^3\Pi_g - c^3\Sigma_u^+$	1174/985	07JoNaRe (Joester et al. 2007), 13ChYeWa (Chan et al. 2013), 13NaEn (Nakajima & Endo 2013), 14NaEn (Nakajima & Endo 2014)
	<i>Fox-Herzberg</i>	$e^3\Pi_g - a^3\Pi_u$	4412/4085	37FoHe (Fox & Herzberg 1937), <i>49Phillips</i> (Phillips 1949), <i>86HaWi</i> (Hardwick & Wini-cur 1986), 98BrHaKoCr (Brockhinke et al. 1998), 17WeKrNaBa (Welsh et al. 2017)
	Herzberg f	$f^3\Sigma_g^+ - a^3\Pi_u$	328/328	69HeLaMa (Herzberg et al. 1969)
	Herzberg g	$g^3\Delta_g - a^3\Pi_u$	436/436	69HeLaMa (Herzberg et al. 1969)
	Krechivska-Schmidt	$3^3\Pi_g - a^3\Pi_u$	133/133	17KrWeBaNa (Krechivska et al. 2017)
	<i>Krechivska-Schmidt</i>	$4^3\Pi_g - a^3\Pi_u$	280/259	15KrBaTrNa (Krechivska et al. 2015) 16KrBaWeNa (Krechivska et al. 2016) 17Kr-WeBaNa (Krechivska et al. 2017)
Quintet				
	<i>Radi-Bornhauser</i>	$1^5\Pi_u - 1^5\Pi_g$	68/63	15BoMaGo (Bornhauser et al. 2015), 17BoViBeKn (Bornhauser et al. 2017)
Intercombination				
		$X^1\Sigma_g^+ - a^3\Pi_u$	16/16	15ChKaBeTa (Chen et al. 2015)
		$1^5\Pi_g - a^3\Pi_u$	70/70	11BoSyKnGe (Bornhauser et al. 2011), 17BoViBeKn (Bornhauser et al. 2017)
		$A^1\Pi_u - b^3\Sigma_g^-$	1/1	15ChKaBeTa (Chen et al. 2015)

bands the $A^1\Pi_u$ state is more connected than the $X^1\Sigma_g^+$ state; this follows from the symmetries of the various states with Π states being most connected.

The separation of the singlet and triplet manifolds becomes more pronounced in the middle sub-figure of Figure 3. This figure also clarifies that vibronic states are strongly interconnected in C_2 , *i.e.*, a given upper state can decay to many different vibrational ground states. These Franck-Condon transitions are numerous due to significant variation in the bond lengths of the different electronic states.

The bottom sub-figure of Figure 3 shows clearly the sparsity of the intercombination bands in contrast to the other observed transitions, yet highlights their importance in connecting the singlet, triplet, and quintet manifolds. The spiral networks of transitions in both the singlet and triplet manifolds are multicoloured as they are between a variety of electronic states, with their linear structure largely determined by angular momentum selection rules $\Delta J = 0, \pm 1$. Note that we have excluded all energy levels and transitions not in the main component from this figure for clarity.

4.2 Updated MARVEL Energy Levels

Figure 4 gives a summary of all 7047 empirical energy levels determined in this study, with each line representing energy levels of a single vibronic state as a function of the total angular momentum quantum number J . These curves are clearly quadratic and smooth, suggesting that there are no major issues with the empirical energy levels.

In Tables 6 to 8, we describe the updated MARVEL dataset for each vibronic level for low-lying singlet states, low-lying triplet states and higher energy states respectively in terms of (a) the range of total angular momentum quantum numbers J and energies included; (b) the total number of quantum states included; (c) the average uncertainty of the derived energies; and (d) the contributing data sources.

Low-lying states, particularly the $X^1\Sigma_g^+(v=0-5)$, $a^3\Pi_u(v=0-6)$, and $A^1\Pi_u(v=0-5)$ ones, are very well characterised to high J values with data from multiple sources leading to low uncertainties usually averaging less than 0.002 cm^{-1} . Higher-lying

[htpb!]

Table 6. Summary of experimentally-derived MARVEL energy levels, including uncertainties and data sources, for low-lying singlet states of $^{12}\text{C}_2$. Bold indicates new data sources, italics indicates updated data sources. No is the number of energy levels in that vibronic state. See Table 5 for the citations to these sources.

State	v	J -range	No	E -range	Av Unc (cm^{-1})	Sources
$X^1\Sigma_g^+$	0	0–74	38	0–9836	0.0019	39Landsver, 63BaRab, 69HeLaMa , 77ChMaMa, 97SoBILiXu, 04ChYeWoLi, 06PeSi, 15ChKaBeTa, 19Nakajima
$X^1\Sigma_g^+$	1	0–72	37	1827–11056	0.0025	39Landsver, 63BaRab, 77ChMaMa, 88DoNiBea, 97SoBILiXu, 04ChYeWoLi, 06PeSi, 15ChKaBeTa, 19Nakajima
$X^1\Sigma_g^+$	2	0–58	30	3627–8105	0.0010	39Landsver, 63BaRab, 77ChMaMa, 88DaAbPh, 88DoNiBea, 97SoBILiXu, 04ChYeWoLi, 15ChKaBeTa, 18KrWeFr
$X^1\Sigma_g^+$	3	0–46	24	5397–9158	0.0021	39Landsver, 63BaRab, 88DaAbPh, 88DoNiBea, 97SoBILiXu, 04ChYeWoLi, 15ChKaBeTa, 18KrWeFr
$X^1\Sigma_g^+$	4	0–40	21	7136–9964	0.0014	88DaAbPh, 88DoNiBea, 95BILiSo, 04ChYeWoLi, 13NaEn, 15ChKaBeTa, 18KrWeFr , 19Nakajima
$X^1\Sigma_g^+$	5	0–30	16	8844–10433	0.0015	88DoNiBea, 13NaEn, 15ChKaBeTa, 18KrWeFr , 19Nakajima
$X^1\Sigma_g^+$	6	0–26	13	10518–11704	0.0044	15ChKaBeTa, 18KrWeFr
$X^1\Sigma_g^+$	7	0–10	6	12155–12339	0.0033	13NaEn, 18KrWeFr
$X^1\Sigma_g^+$	8	0–12	7	13751–14008	0.0051	13NaEn, 18KrWeFr
$X^1\Sigma_g^+$	9	0–12	7	15303–15556	0.0052	13NaEn, 18KrWeFr
$A^1\Pi_u$	0	1–72	72	8272–16541	0.0084	30DiLo , 51Freyemark, 63BaRab, 77ChMaMa, 88DoNiBeb, 88GoCo , 88DaAbPh, 88DoNiBea, <i>16ChKaBeTa</i> , 15ChKaBeTa
$A^1\Pi_u$	1	1–79	77	9856–19657	0.0140	30DiLo , 40HeSu , 51Freyemark, 77ChMaMa, 88DoNiBeb, 88GoCo , 88DaAbPh, 88DoNiBea, 06PeSi, 15ChKaBeTa, <i>16ChKaBeTa</i>
$A^1\Pi_u$	2	1–70	70	11415–19073	0.0023	30DiLo , 40HeSu , 51Freyemark, 77ChMaMa, 88DaAbPh, 88DoNiBeb, 88GoCo , 97SoBILiXu, 04ChYeWoLi, 06PeSi, 15ChKaBeTa, <i>16ChKaBeTa</i>
$A^1\Pi_u$	3	1–75	75	12951–21607	0.0047	30DiLo , 40HeSu , 51Freyemark, 63BaRab, 77ChMaMa, 88DoNiBea, 88GoCo , 97SoBILiXu, 04ChYeWoLi, 15ChKaBeTa, <i>16ChKaBeTa</i>
$A^1\Pi_u$	4	1–74	74	14462–22800	0.0059	40HeSu , 51Freyemark, 63BaRab, 77ChMaMa, 88DoNiBea, 88GoCo , 04ChYeWoLi, 15ChKaBeTa, <i>16ChKaBeTa</i>
$A^1\Pi_u$	5	1–59	59	15949–19784	0.0086	40HeSu , 63BaRab, 88DoNiBea, 04ChYeWoLi, 15ChKaBeTa, <i>16ChKaBeTa</i>
$A^1\Pi_u$	6	1–47	47	17411–20768	0.0085	<i>50Phillips</i> , 63BaRab, 04ChYeWoLi, 15ChKaBeTa, 19Nakajima
$A^1\Pi_u$	7	1–20	20	18849–19469	0.0034	04ChYeWoLi, 15ChKaBeTa
$A^1\Pi_u$	8	2–19	18	20268–20816	0.0047	04ChYeWoLi
$A^1\Pi_u$	9	1–31	30	21650–23080	0.0030	13NaEn, 19Nakajima
$A^1\Pi_u$	10	1–30	30	23013–24338	0.0027	13NaEn, 19Nakajima
$A^1\Pi_u$	11	1–23	22	24352–25128	0.0024	13NaEn, 19Nakajima
$A^1\Pi_u$	12	1–7	6	25665–25740	0.0018	13NaEn
$A^1\Pi_u$	13	1–7	6	26953–27027	0.0018	13NaEn
$A^1\Pi_u$	14	1–5	5	28215–28253	0.0010	13NaEn
$A^1\Pi_u$	15	1–3	3	29452–29465	0.0011	13NaEn
$A^1\Pi_u$	16	1–4	4	30662–30686	0.0019	13NaEn
$B^1\Delta_g$	0	2–47	46	11868–15110	0.0014	88DoNiBeb, <i>16ChKaBeTa</i>
$B^1\Delta_g$	1	2–50	48	13252–16870	0.0016	88DoNiBeb, 89GoCo , <i>16ChKaBeTa</i>
$B^1\Delta_g$	2	2–42	40	14614–17152	0.0014	88DoNiBeb, <i>16ChKaBeTa</i>
$B^1\Delta_g$	3	2–39	37	15953–18120	0.0012	88DoNiBeb, <i>16ChKaBeTa</i>
$B^1\Delta_g$	4	2–36	35	17269–19097	0.0013	88DoNiBeb, <i>16ChKaBeTa</i>
$B^1\Delta_g$	5	2–33	31	18562–20084	0.0016	88DoNiBeb, <i>16ChKaBeTa</i>
$B^1\Delta_g$	6	2–36	32	19833–21616	0.0021	<i>16ChKaBeTa</i>
$B^1\Delta_g$	7	2–34	33	21081–22654	0.0021	<i>16ChKaBeTa</i>
$B^1\Delta_g$	8	3–24	20	22314–23088	0.0032	<i>16ChKaBeTa</i>
$B'^1\Sigma_g^+$	0	0–32	17	15197–16747	0.0008	88DoNiBeb
$B'^1\Sigma_g^+$	1	0–30	16	16617–17974	0.0008	88DoNiBeb
$B'^1\Sigma_g^+$	2	2–28	14	18045–19215	0.0012	88DoNiBeb
$B'^1\Sigma_g^+$	3	0–20	11	19458–20064	0.0011	88DoNiBeb
$B'^1\Sigma_g^+$	4	0–30	16	20878–22208	0.0016	<i>16ChKaBeTa</i>

states generally are characterised by far fewer sources and usually exhibit a much more limited range in J . States with energies lower than approximately $30\,000\text{ cm}^{-1}$ generally retain low median uncertainties on the order of 0.002 cm^{-1} , while the higher-lying states detailed in Table 8 generally have median uncertainties of $0.01–0.1\text{ cm}^{-1}$, reflecting the lower accuracy of ultraviolet-spectroscopy measurements.

4.3 Uncertainties

Figure 5 shows the uncertainties of the energy levels in each electronic state, ordered from left to right in order of increasing energy. The eight low-lying electronic states, $X^1\Sigma_g^+$, $a^3\Pi_u$, $b^3\Sigma_g^-$, $A^1\Pi_u$, $c^3\Sigma_u^+$, $B^1\Delta_g$, $B'^1\Sigma_g^+$, and $d^3\Pi_g$, have uncertainties that range from less than 0.001 cm^{-1} to a small number of transitions with uncertainties greater than 0.01 cm^{-1} . These low uncertainties are definitely suitable for the current needs of high-resolution astronomical spectroscopy. As an example, we note recent trends in using cross-correlation of template and measured spectra to extract

[htpb!]

Table 7. Summary of experimentally-derived MARVEL energy levels, including uncertainties and data sources, for low-lying triplet states of $^{12}\text{C}_2$. Bold indicates new data sources, italics indicates updated data sources. No is the number of energy levels in that vibronic state. See Table 5 for the citations to these sources.

State	v	J -range	No	E -range	Av Unc (cm^{-1})	Sources
$a^3\Pi_u$	0	0–80	226	604–11117	0.0020	69HeLaMa , 79AmChMa, 83Amiot, 85RoWaMiVe, 85SuSaHi, 88DaAbSa, 94PrBe, 98BrHaKoCr, 99LIEw, 06PeSi, 07TaHiAm, 15ChKaBeTa, 17WeKrNaBa
$a^3\Pi_u$	1	0–70	192	2222–9844	0.0020	49Phillips, 79AmChMa, 85CuSa, 85RoWaMiVe, 85YaCuMeCa, 94PrBe, 03KaYaGuYu, 06PeSi, 07TaHiAm, 15ChKaBeTa
$a^3\Pi_u$	2	0–60	173	3816–9563	0.0023	48Phillips, 49Phillips, 79AmChMa, 85RoWaMiVe, 85YaCuMeCa, 94PrBe, 06PeSi, 07TaHiAm, 15ChKaBeTa, 15KrBaTrNa, 17KrWeBa , 17WeKrNaBa
$a^3\Pi_u$	3	0–58	163	5388–10529	0.0059	37FoHe, 48Phillips, 49Phillips, 79AmChMa, 85RoWaMiVe, 85YaCuMeCa, 94PrBe, 07TaHiAm, 10BoKnGe, 15ChKaBeTa, 15KrBaTrNa, 16KrBaWeNa, 17KrWeBa , 17WeKrNaBa
$a^3\Pi_u$	4	0–42	122	6936–9607	0.0061	37FoHe, 48Phillips, 79AmChMa, 86HaWi, 94PrBe, 07TaHiAm, 11BoSyKnGe, 15ChKaBeTa, 17KrWeBa , 17WeKrNaBa
$a^3\Pi_u$	5	0–42	121	8460–11102	0.0233	37FoHe, 48Phillips, 86HaWi, 07TaHiAm, 11BoSyKnGe, 15ChKaBeTa, 17KrWeBa
$a^3\Pi_u$	6	0–36	104	9962–11991	0.0224	37FoHe, 48Phillips, 07TaHiAm, 15ChKaBeTa, 17BoViBeKn , 17KrWeBa
$a^3\Pi_u$	7	0–26	74	11440–12585	0.0076	02TaAm, 07TaHiAm, 14NaEn
$a^3\Pi_u$	8	0–34	100	12894–15210	0.0048	48Phillips, 86HaWi, 02TaAm, 07TaHiAm, 13BoSyKnGe, 13NaEn, 13YeChWa
$a^3\Pi_u$	9	0–35	97	14326–16402	0.0071	48Phillips, 02TaAm, 07TaHiAm, 13NaEn, 13YeChWa
$a^3\Pi_u$	10	0–5	13	15734–15796	0.0022	13NaEn
$a^3\Pi_u$	11	0–7	15	17118–17182	0.0008	13NaEn
$a^3\Pi_u$	12	2–5	6	18479–18509	0.0011	13NaEn
$a^3\Pi_u$	13	1–6	9	19817–19862	0.0016	13NaEn
$a^3\Pi_u$	14	2–5	4	21132–21161	0.0017	13NaEn
$b^3\Sigma_g^-$	0	0–75	106	6250–14542	0.0015	79AmChMa, 85RoWaMiVe, 85YaCuMeCa, 88DaAbSa, 15ChKaBeTa
$b^3\Sigma_g^-$	1	0–70	102	7698–14671	0.0020	79AmChMa, 85RoWaMiVe, 85YaCuMeCa, 15ChKaBeTa
$b^3\Sigma_g^-$	2	0–70	104	9124–16018	0.0018	79AmChMa, 85RoWaMiVe, 85YaCuMeCa, 15ChKaBeTa
$b^3\Sigma_g^-$	3	0–70	99	10528–17342	0.0024	79AmChMa, 85RoWaMiVe, 06PeSi, 15ChKaBeTa
$b^3\Sigma_g^-$	4	2–60	87	11910–16874	0.0026	79AmChMa, 85RoWaMiVe, 06PeSi, 15ChKaBeTa
$b^3\Sigma_g^-$	5	1–58	84	13270–17856	0.0034	79AmChMa, 85RoWaMiVe, 06PeSi, 15ChKaBeTa
$b^3\Sigma_g^-$	6	1–58	80	14608–19140	0.0047	79AmChMa, 15ChKaBeTa
$b^3\Sigma_g^-$	7	2–40	56	15924–18053	0.0047	79AmChMa, 15ChKaBeTa
$b^3\Sigma_g^-$	8	2–30	42	17219–18394	0.0070	15ChKaBeTa
$b^3\Sigma_g^-$	19	17–22	8	30416–30595	0.0100	11BoSyKnGe
$c^3\Sigma_u^+$	0	0–19	25	9280–10006	0.0018	07JoNaRe, 13ChYeWa, 13NaEn
$c^3\Sigma_u^+$	1	0–24	33	11312–12365	0.0018	07JoNaRe, 13ChYeWa, 13NaEn, 14NaEn
$c^3\Sigma_u^+$	2	0–10	14	13315–13482	0.0010	07JoNaRe, 13NaEn
$c^3\Sigma_u^+$	3	0–9	14	15288–15452	0.0006	07JoNaRe, 13NaEn
$c^3\Sigma_u^+$	5	0–5	8	19139–19191	0.0008	13NaEn
$c^3\Sigma_u^+$	6	0–6	9	21015–21065	0.0008	13NaEn
$c^3\Sigma_u^+$	7	0–6	8	22854–22904	0.0008	13NaEn
$d^3\Pi_g$	0	0–81	224	19984–31555	0.0054	48Phillips, 83Amiot, 85CuSa, 94PrBe, 99LIEw, 03KaYaGuYu, 07TaHiAm
$d^3\Pi_g$	1	0–53	159	21738–26809	0.0070	48Phillips, 85SuSaHi, 94PrBe, 07TaHiAm, 13ChYeWa
$d^3\Pi_g$	2	0–41	119	23454–26237	0.0094	48Phillips, 94PrBe, 07TaHiAm, 13ChYeWa, 13NaEn
$d^3\Pi_g$	3	0–39	106	25130–27615	0.0047	07JoNaRe, 07TaHiAm, 13NaEn, 14NaEn, 48Phillips, 94PrBe
$d^3\Pi_g$	4	0–43	126	26761–29736	0.0098	07JoNaRe, 07TaHiAm, 10BoKnGe, 13BoSyKnGe, 13YeChWa
$d^3\Pi_g$	5	0–36	105	28342–30506	0.0051	02TaAm, 07JoNaRe, 07TaHiAm, 13NaEn, 13YeChWa
$d^3\Pi_g$	6	0–35	103	29865–31876	0.0096	02TaAm, 07TaHiAm, 11BoSyKnGe
$d^3\Pi_g$	7	0–34	93	31324–33291	0.0080	02TaAm, 07JoNaRe, 07TaHiAm, 13NaEn
$d^3\Pi_g$	8	0–32	88	32709–34220	0.0216	48Phillips, 07TaHiAm, 13NaEn, 17BoViBeKn
$d^3\Pi_g$	9	2–33	85	34013–35672	0.0106	48Phillips, 07TaHiAm
$d^3\Pi_g$	10	0–34	94	35234–37143	0.0035	48Phillips, 07TaHiAm, 13NaEn
$d^3\Pi_g$	11	1–8	13	36377–36458	0.0015	13NaEn
$d^3\Pi_g$	12	0–9	19	37453–37553	0.0008	13NaEn

very small data signals, e.g. for non-dominant isotopologues (Mollière & Snellen 2019). The quintet states have uncertainties around 0.002 cm^{-1} . In contrast, higher singlet and triplet electronic states have a higher uncertainty, generally $0.01–0.1\text{ cm}^{-1}$, with a smaller spread. These higher uncertainties can be attributed to the lower resolution of the ultraviolet-spectroscopy experiments needed to characterise these high-lying states along with the smaller number of experimental data sources.

It is useful to consider how the source uncertainties of the transitions (illustrated in Figure 2) propagate to the uncertainties of the energy levels (illustrated in Figure 5). Overall, the uncertainty in

the energy levels seems to be approximately an order of magnitude lower than the uncertainty of the transitions. This relationship is explored further in Figure 6, which plots the uncertainty of an energy level (in logarithmic scale) as a function of the number of transitions used in its determination. As expected, in general, as the number of transitions increases the uncertainty of the energy level decreases.

Table 8. Summary of experimentally-derived MARVEL energy levels, including uncertainties and data sources, for highly-excited states of $^{12}\text{C}_2$. Bold indicates new data sources, italics indicates updated data sources. No is the number of energy levels in that vibronic state. See Table 5 for the citations to these sources.

State	ν	J -range	No	E -range	Av Unc (cm^{-1})	Sources
$1^5\Pi_g$	0	0–12	30	29861–30082	0.0047	11BoSyKnGe, 15BoMaGo, 17BoViBeKn
$C^1\Pi_g$	0	1–78	77	34241–44905	0.1054	30DiLo
$C^1\Pi_g$	1	1–71	71	36005–44500	0.0927	30DiLo
$C^1\Pi_g$	2	3–67	64	37719–45336	0.1197	30DiLo
$C^1\Pi_g$	3	1–24	24	39306–40306	0.1532	40HeSu
$C^1\Pi_g$	4	1–36	36	40775–42744	0.1479	40HeSu
$C^1\Pi_g$	5	1–35	35	42033–44909	0.1149	40HeSu
$C^1\Pi_g$	6	1–41	41	43030–45387	0.1543	40HeSu
$C^1\Pi_g$	7	1–37	37	44631–46411	0.1573	<i>50Phillips</i>
$1^5\Pi_u$	0	0–13	35	51651–51920	0.0043	15BoMaGo
$1^5\Pi_u$	1	1–6	11	52495–52553	0.0550	17BoViBeKn
$e^3\Pi_g$	0	1–43	122	40420–42533	0.0471	<i>37FoHe</i> , <i>49Phillips</i> , <i>86HaWi</i> , 17WeKrNaBa
$e^3\Pi_g$	1	1–55	159	41455–44833	0.0421	<i>49Phillips</i> , <i>86HaWi</i> , 98BrHaKoCr, 17WeKrNaBa
$e^3\Pi_g$	2	1–49	143	42433–45059	0.0304	<i>49Phillips</i> , 17WeKrNaBa
$e^3\Pi_g$	3	1–48	138	43366–45832	0.0399	<i>49Phillips</i> , 17WeKrNaBa
$e^3\Pi_g$	4	1–44	123	44260–46291	0.0461	<i>49Phillips</i> , 17WeKrNaBa
$e^3\Pi_g$	5	0–15	41	45120–45349	0.0245	17WeKrNaBa
$e^3\Pi_g$	6	0–16	40	45952–46209	0.0272	17WeKrNaBa
$e^3\Pi_g$	7	0–12	32	46758–46901	0.0268	17WeKrNaBa
$e^3\Pi_g$	8	1–15	40	47541–47787	0.0280	17WeKrNaBa
$e^3\Pi_g$	9	0–14	35	48298–48511	0.0289	17WeKrNaBa
$e^3\Pi_g$	10	0–12	24	49035–49192	0.0289	17WeKrNaBa
$D^1\Sigma_u^+$	0	1–63	32	43231–50457	0.0837	39Landsver, 97SoBILiXu
$D^1\Sigma_u^+$	1	1–65	33	45033–52631	0.0942	39Landsver, 97SoBILiXu
$D^1\Sigma_u^+$	2	1–51	26	46806–51483	0.1091	39Landsver, 97SoBILiXu
$D^1\Sigma_u^+$	3	3–37	18	48569–51014	0.0979	39Landsver, 97SoBILiXu
$D^1\Sigma_u^+$	4	1–41	20	50268–53245	0.0306	95BILiSo, 18KrWeFr
$D^1\Sigma_u^+$	5	1–19	10	51956–52608	0.0169	18KrWeFr
$D^1\Sigma_u^+$	6	1–11	6	53616–53838	0.0250	18KrWeFr
$D^1\Sigma_u^+$	7	1–11	6	55247–55466	0.0276	18KrWeFr
$D^1\Sigma_u^+$	8	1–11	6	56849–57065	0.0321	18KrWeFr
$D^1\Sigma_u^+$	9	1–11	6	58422–58635	0.0101	18KrWeFr
$D^1\Sigma_u^+$	10	1–11	6	59965–60175	0.0101	18KrWeFr
$D^1\Sigma_u^+$	11	1–11	6	61478–61686	0.0091	18KrWeFr
$3^3\Pi_g$	3	1–8	23	50681–50781	0.0743	17KrWeBa
$3^3\Pi_g$	8	1–9	24	54566–54643	0.0918	17KrWeBa
$4^3\Pi_g$	0	1–9	26	52106–52236	0.0696	15KrBaTrNa, 16KrBaWeNa, 17KrWeBa
$4^3\Pi_g$	1	1–8	20	53375–53460	0.0846	15KrBaTrNa, 17KrWeBa
$4^3\Pi_g$	2	1–7	20	54699–54779	0.0836	17KrWeBa
$E^1\Sigma_g^+$	0	0–66	32	54937–62593	0.0610	51Freyemark, 97SoBILiXu
$E^1\Sigma_g^+$	1	0–68	28	56529–64443	0.0655	51Freyemark, 97SoBILiXu
$E^1\Sigma_g^+$	2	4–32	15	58077–59816	0.0863	51Freyemark
$E^1\Sigma_g^+$	3	6–36	13	59550–61658	0.0910	51Freyemark
$E^1\Sigma_g^+$	4	2–46	15	60855–64263	0.0902	51Freyemark
$E^1\Sigma_g^+$	5	10–30	11	62305–63573	0.0787	51Freyemark
$1^1\Delta_u$	0	1–33	61	57374–58868	0.1388	88GoCo , 89GoCo
$1^1\Delta_u$	1	2–37	35	58481–60317	0.1015	88GoCo
$1^1\Delta_u$	2	2–31	30	59546–60814	0.1416	88GoCo
$f^3\Sigma_g^+$	0	3–31	15	70819–72208	0.0843	69HeLaMa
$f^3\Sigma_g^+$	1	5–31	14	72176–73518	0.0819	69HeLaMa
$f^3\Sigma_g^+$	2	3–23	11	73452–74198	0.1053	69HeLaMa
$g^3\Delta_g$	0	3–32	85	72268–73762	0.0789	69HeLaMa
$g^3\Delta_g$	1	3–31	80	73741–75203	0.0833	69HeLaMa
$F^1\Pi_u$	0	10–38	29	74713–76944	0.0994	69HeLaMa
$F^1\Pi_u$	1	2–34	29	76100–78003	0.1099	69HeLaMa

4.4 Differences between old and new MARVEL energy levels

4.4.1 New levels

Considering only the main component, the 2020 MARVEL compilation of $^{12}\text{C}_2$ spectroscopic data added 1524 rovibronic states (765

singlets, 747 triplets, and 12 quintets) to the 2016 compilation and removed 147 states (146 triplets and 1 quintet) due primarily to re-processing of the 07TaHiAm data to remove the predicted unmeasured transitions previously incorrectly included. 55 of the removed states are still present in the 2020 compilation as orphan energy lev-

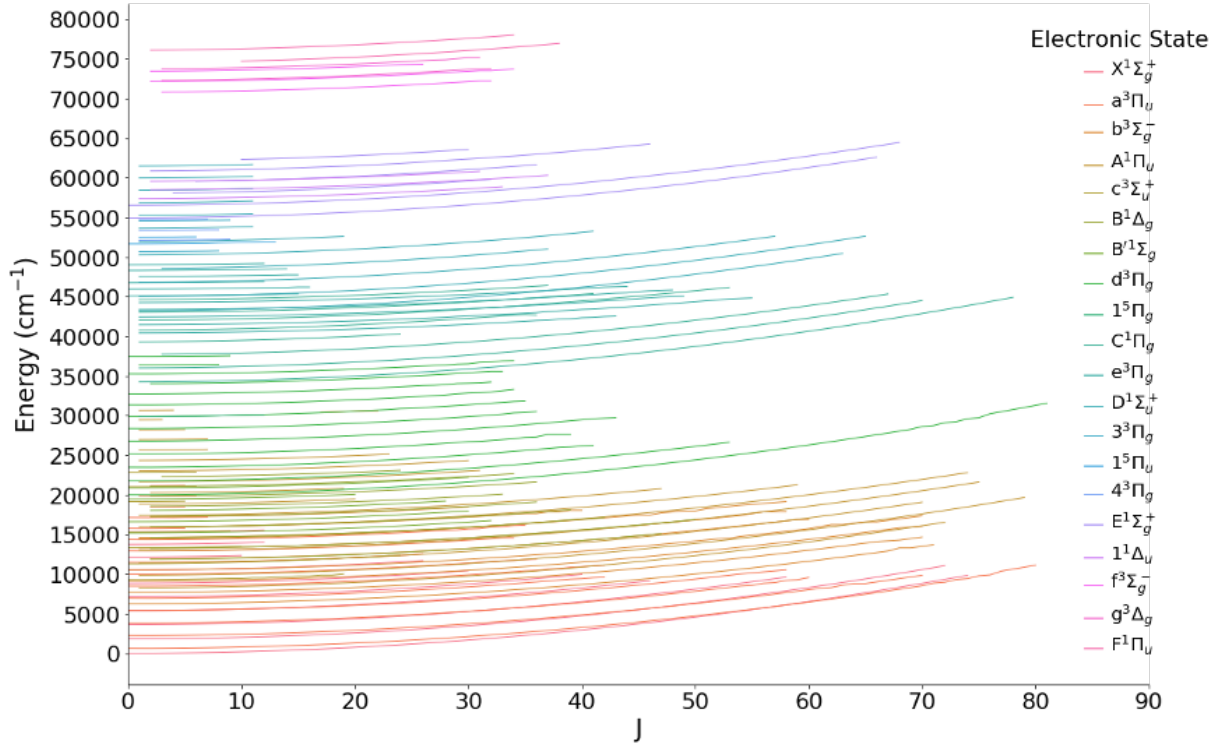


Figure 4. Summary of the energy levels from the MARVEL procedure. Each line is a unique spin-vibronic state, with each electronic state a unique colour.

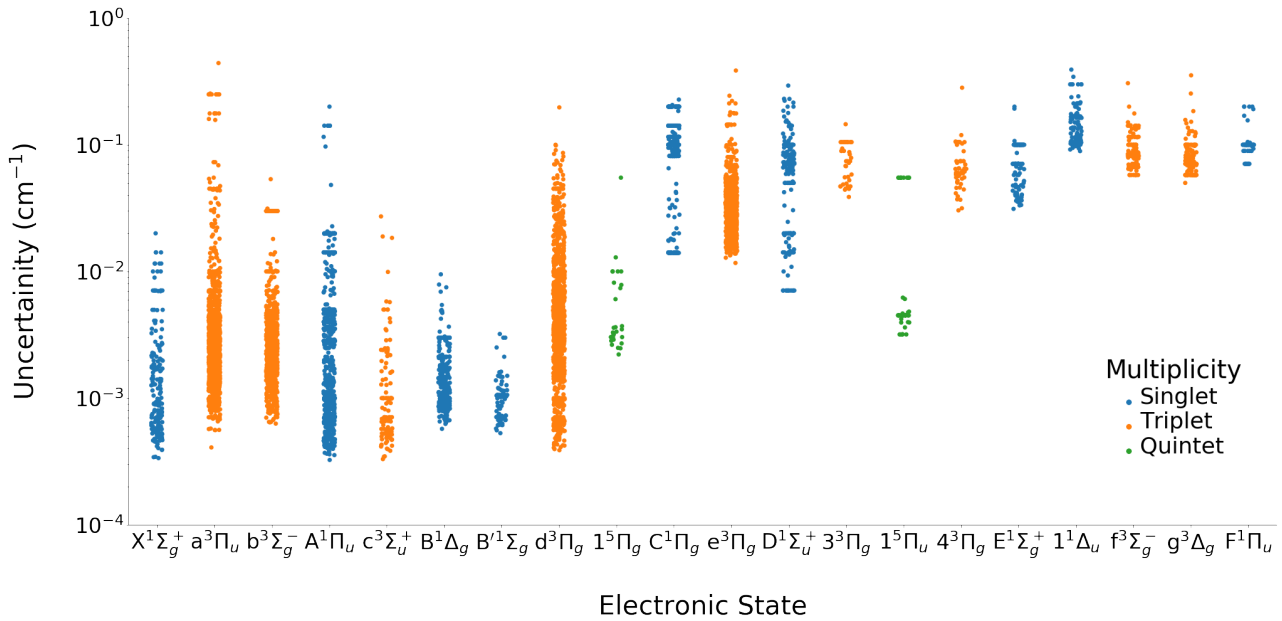


Figure 5. The distribution of uncertainties of the empirical energy levels generated for each electronic energy level.

els (*i.e.*, outside the main spectroscopic network), indicating that the connections between these energy levels and the main component were removed by the reprocessing.

The new energy levels span 18 of the total of 20 electronic states in the 2020 MARVEL $^{12}\text{C}_2$ spectroscopic data compilation, and 79 of the 142 vibronic states. Six of these electronic states ($\text{C}^1\Pi_g$, $\text{F}^1\Pi_u$, $\text{f}^3\Sigma_g^+$, $\text{g}^3\Delta_g$, $1^1\Delta_u$, $3^3\Pi_g$) and 44 of these vi-

bronic states are entirely new to this 2020 update. Increases in coverage were also notable for the $\text{e}^3\Pi_g$ state (increase of 333 levels across 11 vibrational states) and the $\text{A}^1\Pi_u$ state (increase of 106 levels across 12 vibrational states).

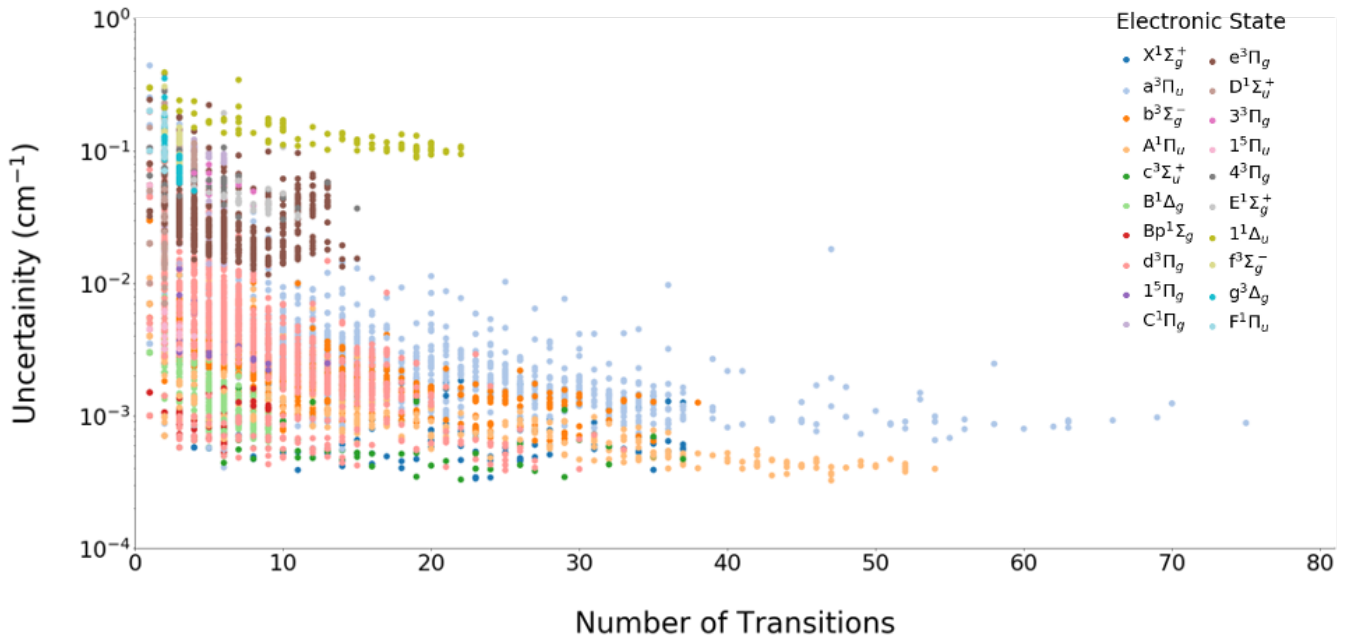


Figure 6. The relationship between the final uncertainty of the empirical energy levels and the number of transitions that contributed to the derived energy level.

□

Table 9. Differences between old and new MARVEL compilations by electronic state, quantified by MAD (mean absolute deviation) and Max (maximum deviation). The "No" column specifies the number of states common to the new and old compilations.

State	No	2020 – 2016 Energies		2016 Av unc
		MAD	Max	
X $^1\Sigma_g^+$	174	0.0034	0.0565	0.0006
A $^1\Pi_u$	512	0.0041	0.0566	0.0022
B $^1\Delta_g$	322	0.0013	0.0565	0.0022
B' $^1\Sigma_g^+$	58	0.0006	0.0019	0.0008
D $^1\Sigma_u^+$	117	0.0888	0.5387	0.1643
E $^1\Sigma_g^+$	113	0.0140	0.4942	0.1498
a $^3\Pi_u$	1381	0.0386	3.0007	0.0017
b $^3\Sigma_g^-$	762	0.0079	0.0829	0.0016
c $^3\Sigma_u^+$	111	0.0038	0.0152	0.0015
d $^3\Pi_g$	1314	0.0847	7.8451	0.0023
e $^3\Pi_g$	563	0.0498	1.4348	0.0659
4 $^3\Pi_g$	32	0.4383	1.4070	0.0863
1 $^5\Pi_g$	29	0.0067	0.0252	0.0116
1 $^5\Pi_u$	35	0.0065	0.0252	0.0171

4.4.2 Changes in energy in previously included levels

The old (2016) and new (2020) MARVEL rovibronic energy levels for $^{12}\text{C}_2$ are different, though these differences are usually small. This difference is quantified in Table 9, which presents the average change in the energy levels of a given electronic state for quantum states that are in both the 2016 and this 2020 MARVEL compilations. The same data at vibronic resolution is provided in the Supplementary Information.

Usually, the two MARVEL compilations predict energies that on average agree to about 0.005 cm^{-1} for low-lying states, with maximum deviations around 0.06 cm^{-1} . For higher electronic

states, the differences in empirical energies between the two compilations is higher, up to an average of 0.44 cm^{-1} for the 4 $^3\Pi_g$ state following the addition of significant new data in this 2020 MARVEL update. The main outliers to this trend are the a $^3\Pi_u$, d $^3\Pi_g$, and e $^3\Pi_g$ states, which all have quite sizeable modifications from 2016 to 2020. These changes can be traced primarily to a reprocessing of the 49Phillips and 07TaHiAm data, which corrected earlier errors. We carefully examined the states with large deviations and found that the energies along a vibronic band were far smoother and more reasonable in the 2020 update than the original 2016 compilation, indicating that these modifications improved the overall data compilation.

An integral part of the MARVEL process is to provide predictions for the accuracy of its empirical energy levels. Our data here shows that the 2016 prediction of the average uncertainties generally is quite close to the changes in energy observed between the 2016 and 2020 compilation, indicating that the original uncertainties were reasonable. The most notable underestimation in the original uncertainties is for the X $^1\Sigma_g^+$ state, which under-predicted changes by about a factor of 5. Other significant deviations between the 2016 prediction uncertainties and the 2020–2016 changes in energy can be attributed to mis-assignments and processing errors in the 2016 compilation.

5 UPDATED C_2 LINE LISTS

The supplementary information of this paper contains three updated states files for $^{12}\text{C}_2$, $^{12}\text{C}^{13}\text{C}$ and $^{13}\text{C}_2$ called 12C2_8states_MARVEL-2020.states, 12C-13C_8states_MARVEL-2020.states and 13C2_8states_MARVEL-2020.states respectively.

The main modification to the original 8states $^{12}\text{C}_2$ line list states file is that we re-MARVELised the energy levels by replacing existing energy levels with 4842 MARVELised energy levels from

this 2020 MARVEL update; these MARVELised energy levels are denoted by a "m" while energy levels computed solely from the DUO spectroscopic model are denoted by "d". Note that there has been no modifications to the underlying spectroscopic model of this line list, *i.e.*, the potential energy and coupling curves were not refitted. For full details of the spectroscopic model for this linelist, one should refer to the original line-list paper (Yurchenko et al. 2018b).

Though we haven't compiled a MARVEL dataset for the C₂ isotopologues, a reasonable assumption is that the line list errors are similar between different isotopologues. Therefore, we follow past precedent (Polyansky et al. 2017; McKemmish et al. 2019) in creating a pseudo-MARVELised states file for ¹²C¹³C and ¹³C₂ by using:

$$E_{\text{iso}} \approx E_{\text{iso}}^{\text{Duo}} + (E_{\text{main}}^{\text{MARVEL}} - E_{\text{main}}^{\text{Duo}}), \quad (1)$$

where E_{iso} is the isotopologue energy for a given state in the final line list, $E_{\text{iso}}^{\text{Duo}}$ is the original spectroscopic model prediction using DUO and $E_{\text{main}}^{\text{MARVEL}}$ and $E_{\text{main}}^{\text{Duo}}$ are the MARVEL and DUO predicted energies of the state for the main isotopologue, in the case ¹²C₂. Energy levels modified in this way are labelled by "i" (for isotopologue pseudo-MARVELisation, in this way clearly distinguished from MARVELisation in the main isotopologue states file). For the case of C₂, nuclear spin statistics means that some microstates are present in the isotopologue states files that are not present in the main ¹²C₂ isotopologue states file, e.g. only one parity component in a Π state is retained for each J in ¹²C₂ while both are present for ¹³C₂ and ¹²C¹³C. To account for this, we used (MARVEL - DUO) energy differences from a single ¹²C₂ parity state to correct both parity states in the isotopologue files.

The minor modification to the 8states ¹²C₂ states file is the inclusion of 71 energy levels that were predicted by 07TaHiAm data but not otherwise included. These were based on 746 transition frequencies from 07TaHiAm (Tanabashi et al. 2007) which were predicted (not experimentally measured), with some of these inadvertently included in the 2016 compilation though none are in this update. Given that the 07TaHiAm predictions are based on band-specific fits, they are likely more accurate than the original 8states energy levels. Therefore, we found the associated energy levels of these additional lines by creating an extended MARVEL input transitions file with these 746 additional frequencies (called 12C2_experimentaland07TaHiPredicted_Marvel.inp in the Supplementary Information) and extracted 71 additional energy levels (compiled in Predicted07TaHiAm.energies file in the Supplementary Information) which replaced the original energy levels in our updated ¹²C₂ 8states states file, with a label "p" (for perturbed).

Note that the process of MARVELising the 8states linelist was shown to help identify very subtle mistakes in the MARVEL compilation itself. For example, large errors in X ¹Σ_g⁺, $v = 2$, $J = 50 - 54$ energies between the line-list prediction and MARVEL energies helped identify a digitisation error where a "8" was read as a "3" in the transition 77ChMaMa.558. These errors were corrected in the final set of MARVEL transitions, energy levels and line lists provided by the Supplementary Information.

As detailed in Table 10, this update increases the number of MARVELised energy levels within the line list from 4555 to 4916, increasing the coverage from 10.3% of all rovibronic levels to 11.1%. The new MARVELised energy levels are primarily additional vibrational levels ($v = 8 - 9, 11 - 16$) and expanded rotational coverage within the A ¹Π_u state, with data on b ³Σ_g⁻, $n = 19$ also being added for the first time. The total number of transi-

Table 10. Summary of the overall proportion of energy levels and transitions that are MARVELised, *i.e.* based entirely on experimentally-derived MARVEL energy levels.

	8states	
	Original	Update
Energy levels		
Number MARVELised	4 555	4 916*
Total	44 189	44 189
% MARVELised	10.3	11.1
All transitions (no intensity threshold)		
Number MARVELised	258 729	307 076
Total Num	6 080 920	6 080 920
% MARVELised	4.3	5.0

* 71 of these MARVELised energy levels are found by combining the 07TaHiAm predicted transition frequencies with the other MARVEL energy levels and running MARVEL.

tions that are MARVELised, *i.e.*, those with frequencies which are entirely determined by MARVEL energy levels, remains relatively low, increasing from 4.3% to 5.2%.

Looking at the strong to medium intensity transitions, however, in Figure 7, we see that the bulk of the strong transitions are MARVELised and that the 2020 update increases the percentage of MARVELised transitions by about 5% when considering the percentage of transitions with intensities above $10^{-17} - 10^{-24}$ cm molecule⁻¹ at 1000 K. The updated line list now has experimentally-derived (MARVELised) transition frequencies for all strong transitions with intensities above 10^{-17} cm molecule⁻¹ (from 95.6% in original 8states) and 80.0% (from 75.7%) of all transitions with intensities above 10^{-22} cm molecule⁻¹ at 1000 K.

Due to the very high proportion of MARVELisation for strong-to moderate-strength transitions across the line list's full spectral range, this updated ¹²C₂ line list is suitable for cross-correlation high-resolution studies of ¹²C₂ in gaseous astrochemistry environments such as exoplanets (de Kok et al. 2014).

6 DISCUSSION AND CONCLUSIONS

The 2016 MARVEL compilation has been significantly updated, with the addition of assigned transitions data from 8 old and 5 new experiments on ¹²C₂ to significantly extend the previous MARVEL dataset for ¹²C₂, including an extra 8072 transitions and 1524 energy levels spanning an extra six electronic states, and extra 44 vibronic states. Data from five previously included sources have been updated and extended. The new data enabled a significant improvement to the quality of the ExoMol ¹²C₂ linelist by increasing the MARVELisation-fraction of strong lines with frequencies above 10^{-18} cm molecule⁻¹ from 94.2% to 99.4%. This increase in high accuracy experimentally-derived (*i.e.*, MARVEL) energy levels is extremely important astrophysically for very high resolution cross-correlation measurements that are now increasingly common with the new generation of ground-based ultra-large telescopes.

For laboratory spectroscopists, the existence of the MARVEL compilation, the MARVEL procedure and line lists have two main benefits: (1) a method to validate their data - for example, in this paper, use of MARVEL enables calibration errors in 17KrWeBa to be identified and corrected, (2) enables their new results to be readily available to applications experts. Inclusion of new data is best enabled by producing formatted assigned transitions, ideally

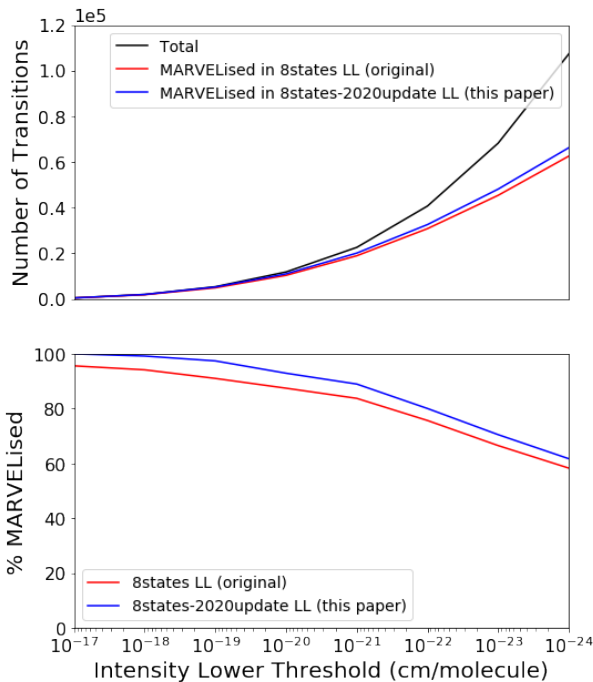


Figure 7. Proportion of strong-to-moderate intensity transitions that are MARVELised (based on experimentally-derived MARVEL energy levels) at 1000 K in the updated line list compared to the original `8states` line list. Top panel considers the number of transitions (total number of transitions vs the number MARVELised in the original and new versions of the line list), whereas the bottom panel converts this to percentage of transitions that are MARVELised. The horizontal axis of both panels is an intensity lower threshold in a logarithmic scale; the vertical axis data gives data for all transitions with intensities above this threshold.

adding their new data to pre-existing MARVEL compilations for the molecule and contacting the creators of the most recent line list for their molecule. This strongly emphasizes the importance of authors providing their primary experimental data in the form of assigned line lists rather than just supplying compound results such as spectroscopic constants. MARVEL compilations currently exist for AlH (Yurchenko et al. 2018a), BeH (Darby-Lewis et al. 2018), $^{12}\text{C}_2$ (Furtenbacher et al. 2016), ^{14}NH (Darby-Lewis et al. 2019a), NO (Wong et al. 2017), $^{16}\text{O}_2$ (Furtenbacher et al. 2019), $^{48}\text{Tl}^{16}\text{O}$ (McKemmish et al. 2017), $^{90}\text{Zr}^{16}\text{O}$ (McKemmish et al. 2018), isotopologues of H_2O (Tennyson et al. 2009, 2010, 2013, 2014b,a; Clark et al. 2020), H_2^{32}S (Chubb et al. 2018b), isotopologues of H_3^+ (Furtenbacher et al. 2013a,b), isotopologues of SO_2 (Tóbiás et al. 2018), C_2H_2 (Chubb et al. 2018a), H_2CCO (Fábri et al. 2011) and NH_3 (Al Derzi et al. 2015; Coles et al. 2020), with ongoing work on other molecules.

For many diatomics accurate measurement of spin-forbidden bands is very important for enabling the relative positioning of the spin manifolds, in the present case the singlet, triplet and quintet ones. There are 88 of these transitions known for $^{12}\text{C}_2$; however, the small T_e of the lowest singlet state ($\approx 600\text{ cm}^{-1}$) increases the importance of this information as this means that triplet absorption is very important for the high-resolution spectroscopy of C_2 .

All allowed electronic bands from states below 12000 cm^{-1} to a known electronic state have rotationally resolved data included in this MARVEL update except for the Messerle–Krauss band and the Kable–Schmidt band. In the former case, the initial assignment of the band is currently being questioned (Nauta & Schmidt 2020)

with the $\text{C}'\ ^1\Pi_g$ expected by theory to be much higher in energy. In the latter case, the two electronic states involved are well characterised by other studies and so the updated `8states` ExoMol line list can be expected to provide very accurate predictions of its spectroscopy for users.

A common trait of the higher lying states is the higher uncertainties in their energies, originating from lower resolution studies in the ultraviolet region than other visible region studies. Of particular note is the Deslandres–d’Azambuja band system which has been seen in flames (Hornbeck & Herman 1949), plasma plumes (Camacho et al. 2008), laser ablation of graphite (Acquaviva & De Giorgi 2002) and astrophysics (Gredel et al. 1989; Berdyugina et al. 2007). Yet remarkably the only modern, high resolution study of these band was made of $^{13}\text{C}_2$ (Antić-Jovanović et al. 1985). A high resolution study of the Deslandres–d’Azambuja bands for $^{12}\text{C}_2$ is overdue.

ACKNOWLEDGMENTS

We thank Klaas Nauta, Tim Schmidt and Scott Kable for helpful discussions and feedback. SNY and JT’s work was supported by the STFC Projects No. ST/M001334/1 and ST/R000476/1. The work performed in Budapest received support from NKFIH (grant no. K119658) and from the ELTE Excellence Program (1783-3/2018/FEKUTSTRAT) supported by the Hungarian Ministry of Human Capacities (EMMI).

DATA AVAILABILITY STATEMENT

The data underlying this article are available in the article and in its online supplementary material. These include the following file;

- README_2020_C2_MARVEL - Explanation of all files within the SI
- 12C2_MARVEL.inp - The final MARVEL transitions file
- 12C2_MARVEL.energies - The final MARVEL energies file
- 12C2_experimentalplus07TaHiAmpredicted_MARVEL.inp - The MARVEL input file that allows the predictions of 07TaHiAm to be incorporated into the final line list
- Predicted07TaHiAm.energies - The additional energies predicted from 12C2_experimentalplus07TaHiAmpredicted_MARVEL.inp
- 12C2__8states_MARVEL-2020.states, 12C13C__8states_MARVEL-2020.states and 13C2__8states_MARVEL-2020.states - The updated states file for the ExoMol 8states line list (to be used with trans file from ExoMol website)
- SI_2020_C2MARVEL.pdf - Expanded analysis tables and figures

REFERENCES

- Acquaviva S., De Giorgi M. L., 2002, *Appl. Surf. Sci.*, 197, 21
 Al Derzi A. R., Furtenbacher T., Yurchenko S. N., Tennyson J., Császár A. G., 2015, *J. Quant. Spectrosc. Radiat. Transf.*, 161, 117
 Amiot C., 1983, *Astrophys. J. Suppl.*, 52, 329
 Amiot C., Chauville J., Maillard J.-P., 1979, *J. Mol. Spectrosc.*, 75, 19
 Antić-Jovanović A., Bojović V., Pešić D. S., Vujisić B. R., Rakotoarijimy D., Weniger S., 1985, *J. Mol. Spectrosc.*, 110, 86
 Árendás P., Furtenbacher T., Császár A. G., 2016, *J. Math. Chem.*, 54, 806

- Asplund M., Grevesse N., Sauval A. J., Prieto C. A., Blomme R., 2005, *Astron. Astrophys.*, 431, 693
- Babb J. F., Smyth R. T., McLaughlin B. M., 2019, *Astrophys. J.*, 876, 38
- Ballik E. A., Ramsay D. A., 1963, *Astrophys. J.*, 137, 84
- Berdugina S. V., Berdugina A. V., Pirola V., 2007, *Phys. Rev. Lett.*, 99, 091101
- Birkby J., de Kok R., Brogi M., Schwarz H., Albrecht S., de Mooij E., Snellen I., 2013, *The Messenger*, 154, 57
- Blunt V. M., Lin H., Sorkhabi O., Jackson W. M., 1995, *J. Mol. Spectrosc.*, 174, 274
- Bornhauser P., Knopp G., Gerber T., Radi P. P., 2010, *J. Mol. Spectrosc.*, 262, 69
- Bornhauser P., Sych Y., Knopp G., Gerber T., Radi P. P., 2011, *J. Chem. Phys.*, 134, 044302
- Bornhauser P., Sych Y., Knopp G., Gerber T., Radi P. P., 2013, *Chem. Phys. Lett.*, 572, 16
- Bornhauser P., Marquardt R., Gourlaouen C., Knopp G., Beck M., Gerber T., van Bokhoven J. A., Radi P. P., 2015, *J. Chem. Phys.*, 142, 094313
- Bornhauser P., Visser B., Beck M., Knopp G., van Bokhoven J. A., Marquardt R., Radi P. P., 2017, *J. Chem. Phys.*, 146, 114309
- Braut J. W., Delbouille L., Grevesse N., Roland G., Sauval A. J., Testerman L., 1982, *Astron. Astrophys.*, 108, 201
- Brockhinke A., Hartlieb A. T., Kohse-Hoinghaus K., Crosley D. R., 1998, *Appl. Phys. B*, 67, 659
- Camacho J. J., Diaz L., Santos M., Reyman D., Poyato J. M. L., 2008, *J. Phys.D: Appl. Phys.*, 41
- Chan M.-C., Yeung S.-H., Wong Y.-Y., Li Y., Chan W.-M., Yim K.-H., 2004, *Chem. Phys. Lett.*, 390, 340
- Chan M.-C., Yeung S.-H., Wang N., Cheung A. S.-C., 2013, *J. Phys. Chem. A*, 117, 9578
- Chauville J., Maillard J. P., Mantz A. W., 1977, *J. Mol. Spectrosc.*, 68, 399
- Chen W., Kawaguchi K., Bernath P. F., Tang J., 2015, *J. Chem. Phys.*, 142, 064317
- Chen W., Kawaguchi K., Bernath P. F., Tang J., 2016, *J. Chem. Phys.*, 144, 064301
- Chubb K. L., et al., 2018a, *J. Quant. Spectrosc. Radiat. Transf.*, 204, 42
- Chubb K. L., et al., 2018b, *J. Quant. Spectrosc. Radiat. Transf.*, 218, 178
- Clark V. H. J., Owens A., Tennyson J., Yurchenko S. N., 2020, *J. Quant. Spectrosc. Radiat. Transf.*
- Coles P. A., Tennyson J., Yurchenko S. N., Furtenbacher T., Tóbiás R., Császár A. G., 2020, *J. Quant. Spectrosc. Radiat. Transf.*
- Császár A. G., Furtenbacher T., 2011, *J. Mol. Spectrosc.*, 266, 99
- Császár A. G., Czako G., Furtenbacher T., Mátyus E., 2007, *Annu. Rep. Comput. Chem.*, 3, 155
- Császár A. G., Furtenbacher T., Árendás P., 2016, *J. Phys. Chem. A*, 120, 8949
- Curtis M., Sarre P., 1985, *J. Mol. Spectrosc.*, 114, 427
- Darby-Lewis D., Tennyson J., Lawson K. D., Yurchenko S. N., Stamp M. F., Shaw A., Brezinsek S., JET Contributor 2018, *J. Phys. B: At. Mol. Opt. Phys.*, 51, 185701
- Darby-Lewis D., et al., 2019b, *J. Mol. Spectrosc.*, 362, 69
- Darby-Lewis D., et al., 2019a, *J. Mol. Spectrosc.*, 362, 69
- Davis S. P., Phillips J. G., Rao M. L. P., Abrams M. C., 1988, *J. Opt. Soc. Am. B*, 5, 2280
- Dieke G. H., Lochte-Holtgreven W., 1930, *Zeitschrift für Physik*, 62, 767
- Douay M., Nietmann R., Bernath P. F., 1988a, *J. Mol. Spectrosc.*, 131, 250
- Douay M., Nietmann R., Bernath P. F., 1988b, *J. Mol. Spectrosc.*, 131, 261
- Fábri C., Mátyus E., Furtenbacher T., Nemes L., Mihály B., Zoltáni T., Császár A. G., 2011, *J. Chem. Phys.*, 135, 094307
- Fox J. G., Herzberg G., 1937, *Phys. Rev.*, 52, 638
- Freymark H., 1951, *Annalen der Physik*, 8, 221
- Furtenbacher T., Császár A. G., 2012a, *J. Quant. Spectrosc. Radiat. Transf.*, 113, 929
- Furtenbacher T., Császár A. G., 2012b, *J. Molec. Struct. (THEOCHEM)*, 1009, 123
- Furtenbacher T., Császár A. G., Tennyson J., 2007, *J. Mol. Spectrosc.*, 245, 115
- Furtenbacher T., Szidarovszky T., Mátyus E., Fábri C., Császár A. G., 2013a, *J. Chem. Theory Comput.*, 9, 5471
- Furtenbacher T., Szidarovszky T., Fábri C., Császár A. G., 2013b, *Phys. Chem. Chem. Phys.*, 15, 10181
- Furtenbacher T., Árendás P., Mellau G., Császár A. G., 2014, *Sci. Rep.*, 4, 4654
- Furtenbacher T., Szabó I., Császár A. G., Bernath P. F., Yurchenko S. N., Tennyson J., 2016, *Astrophys. J. Suppl.*, 224, 44
- Furtenbacher T., Horváth M., Koller D., Sólyom P., Balogh A., Balogh I., Császár A. G., 2019, *J. Phys. Chem. Ref. Data*, 48, 023101
- Goebel J. H., Bregman J. D., Cooper D. M., Goorvitch D., Langhoff S. R., Witteborn F. C., 1983, *Astrophys. J.*, 270, 190
- Goodwin P. M., Cool T. A., 1988, *J. Chem. Phys.*, 89, 6600
- Goodwin P. M., Cool T. A., 1989, *J. Mol. Spectrosc.*, 133, 230
- Goorvitch D., 1990, *Astrophys. J. Suppl.*, 74, 769
- Gredel R., van Dishoeck E. F., Black J. H., 1989, *Astrophys. J.*, 338, 1047
- Gredel R., Black J. H., Yan M., 2001, *Astron. Astrophys.*, 375, 553
- Hall P. B., Maxwell A. J., 2008, *Astrophys. J.*, 678, 1292
- Hardwick J. L., Winicur D. H., 1986, *J. Mol. Spectrosc.*, 115, 175
- Herzberg G., Sutton R. B., 1940, *Can. J. Res.*, 18a, 74
- Herzberg G., Lagerqvist A., Malmberg C., 1969, *Can. J. Phys.*, 47, 2735
- Hornbeck G. A., Herman R. C., 1949, *J. Chem. Phys.*, 17, 842
- Iglesias-Groth S., 2011, *Mon. Not. R. Astron. Soc.*, 411, 1857
- Joester J. A., Nakajima M., Reilly N. J., Kokkin D. L., Nauta K., Kable S. H., Schmidt T. W., 2007, *J. Chem. Phys.*, 127, 214303
- Kaminski C. F., Hughes I. G., Ewart P., 1997, *J. Chem. Phys.*, 106, 5324
- Kaniki J., Yang X. H., Guo Y. C., Yu S. S., Li B. X., Liu Y. Y., Chen Y. Q., 2003, *Prog. Nat. Sci.*, 13, 736
- Kowalski P. M., 2010, *Astron. Astrophys.*, 519, L8
- Krechivska O., Bacskay G. B., Troy T. P., Nauta K., Kreuscher T. D., Kable S. H., Schmidt T. W., 2015, *J. Phys. Chem. A*, 119, 12102
- Krechivska O., Bacskay G. B., Welsh B. A., Nauta K., Kable S. H., Stanton J. F., Schmidt T. W., 2016, *J. Chem. Phys.*, 144, 144305
- Krechivska O., Welsh B. A., Fréreau J., Nauta K., Kable S. H., Schmidt T. W., 2018, *J. Mol. Spectrosc.*, 344, 1
- Krechivska O., Welsh B. A., Bacskay G. B., Nauta K., Kable S. H., Schmidt T. W., 2017, *J. Chem. Phys.*, 146, 134306
- Lambert D. L., Sheffer Y., Danks A. C., Arpigny C., Magain P., 1990, *Astrophys. J.*, 353, 640
- Landsverk O. G., 1939, *Phys. Rev.*, 56, 769
- Lebourlot J., Roueff E., 1986, *J. Mol. Spectrosc.*, 120, 157
- Lloyd G. M., Ewart P., 1999, *J. Chem. Phys.*, 110, 385
- Macrae R. M., 2016, *Science progress*, 99, 1
- McKemmish L. K., et al., 2017, *Astrophys. J. Suppl.*, 228, 15
- McKemmish L. K., et al., 2018, *Astrophys. J.*, 867, 33
- McKemmish L. K., Masseron T., Hoeijmakers J., Pérez-Mesa V. V., Grimm S. L., Yurchenko S. N., Tennyson J., 2019, *Mon. Not. R. Astron. Soc.*, 488, 2836
- Messerle G., 1967, PhD thesis, Technischen Hochschule Munchen
- Messerle G., Krauss L., 1967, *Z. Naturforschung A*, A 22, 2015
- Mollière P., Snellen I., 2019, *Astronomy & Astrophysics*, 622, A139
- Nakajima M., 2019, *J. Mol. Spectrosc.*, 355, 14
- Nakajima M., Endo Y., 2014, *J. Mol. Spectrosc.*, 302, 9
- Nakajima M., Endo Y., 2013, *J. Chem. Phys.*, 139, 244310
- Nakajima M., Joester J. A., Page N. I., Reilly N. J., Bacskay G. B., Schmidt T. W., Kable S. H., 2009, *J. Chem. Phys.*, 131, 044301
- Nauta K., 2020, personal communication
- Nauta K., Schmidt T., 2020, personal communication
- Petrova T., Sinitsa L., 2006, *Opt. Spectrosc.*, 101, 871
- Phillips J. G., 1948a, *Astrophys. J.*, 107, 387
- Phillips J. G., 1948b, *Astrophys. J.*, 107, 399
- Phillips J. G., 1949, *Astrophys. J.*, 110, 73
- Phillips J. G., 1950, *Astrophys. J.*, 112, 131
- Polyansky O. L., Kyuberis A. A., Lodi L., Tennyson J., Ovsyannikov R. I., Zobov N., 2017, *Mon. Not. R. Astron. Soc.*, 466, 1363
- Prasad C. V. V., Bernath P. F., 1994, *Astrophys. J.*, 426, 812
- Rao N. K., Lambert D. L., 2008, *Mon. Not. R. Astron. Soc.*, 384, 477

- Rousselot R., Hill S. M., Burger M. H., Brain D. A., Laffont C., Moreels G., 2000, *Icarus*, 146, 263
- Roux F., Wannous G., Michaud F., Verges J., 1985, *J. Mol. Spectrosc.*, 109, 334
- Schmidt T. W., Bacskay G. B., 2011, *J. Chem. Phys.*, 134, 224311
- Sonnentrucker P., Welty D. E., Thorburn J. A., York D. G., 2007, *Astrophys. J. Suppl.*, 168, 58
- Sorkhabi O., Blunt V. M., Lin H., Xu D., Wrobel J., Price R., Jackson W. M., 1997, *J. Chem. Phys.*, 107, 9842
- Suzuki T., Saito S., Hirota E., 1985, *J. Mol. Spectrosc.*, 113, 399
- Swan W., 1857, *Trans. R. Soc. Edinburgh*, 21, 411
- Swings P., 1943, *Mon. Not. R. Astron. Soc.*, 103, 86
- Tanabashi A., Amano T., 2002, *J. Mol. Spectrosc.*, 215, 285
- Tanabashi A., Hirao T., Amano T., Bernath P. F., 2007, *Astrophys. J. Suppl.*, 169, 472
- Tennyson J., Yurchenko S. N., 2012, *Mon. Not. R. Astron. Soc.*, 425, 21
- Tennyson J., et al., 2009, *J. Quant. Spectrosc. Radiat. Transf.*, 110, 573
- Tennyson J., et al., 2010, *J. Quant. Spectrosc. Radiat. Transf.*, 111, 2160
- Tennyson J., et al., 2013, *J. Quant. Spectrosc. Radiat. Transf.*, 117, 29
- Tennyson J., et al., 2014a, *Pure Appl. Chem.*, 86, 71
- Tennyson J., et al., 2014b, *J. Quant. Spectrosc. Radiat. Transf.*, 142, 93
- Tóbiás R., Furtenbacher T., Császár A. G., Naumenko O. V., Tennyson J., Flaud J.-M., Kumard P., Poirier B., 2018, *J. Quant. Spectrosc. Radiat. Transf.*, 208, 152
- Tóbiás R., Furtenbacher T., Tennyson J., Császár A. G., 2019, *Phys. Chem. Chem. Phys.*, 21, 3473
- Tóbiás R., et al., 2020, *Nat. Commun.*, 11, 1708
- Visser B., Beck M., Bornhauser P., Knopp G., van Bokhoven J. A., Radi P., Gourlaouen C., Marquardt R., 2019, *Mol. Phys.*, 0, 1
- Wehres N., Romanzin C., Linnartz H., Van Winckel H., Tielens A. G. G. M., 2010, *Astron. Astrophys.*, 518, A36
- Welsh B. A., Krechkivska O., Nauta K., Bacskay G. B., Kable S. H., Schmidt T. W., 2017, *J. Chem. Phys.*, 147, 024305
- Wollaston W. H., 1802, *Phil. Trans. R. Soc. Lond.*, 92, 365
- Wong A., Yurchenko S. N., Bernath P., Mueller H. S. P., McConkey S., Tennyson J., 2017, *Mon. Not. R. Astron. Soc.*, 470, 882
- Yan W.-B., Curl R., Merer A. J., Carrick P. G., 1985, *J. Mol. Spectrosc.*, 112, 436
- Yeung S.-H., Chan M.-C., Wang N., Cheung A. S.-C., 2013, *Chem. Phys. Lett.*, 557, 31
- Yurchenko S. N., Lodi L., Tennyson J., Stolyarov A. V., 2016, *Comput. Phys. Commun.*, 202, 262
- Yurchenko S. N., Williams H., Leyland P. C., Lodi L., Tennyson J., 2018a, *Mon. Not. R. Astron. Soc.*, 479, 1401
- Yurchenko S. N., Szabó I., Pyatenko E., Tennyson J., 2018b, *Mon. Not. R. Astron. Soc.*, 480, 3397
- de Kok R. J., Birkby J., Brogi M., Schwarz H., Albrecht S., de Mooij E. J., Snellen I. A., 2014, *Astronomy & Astrophysics*, 561, A150

This paper has been typeset from a $\text{\TeX}/\text{\LaTeX}$ file prepared by the author.